Lawrence Berkeley National Laboratory
Recent Work

Title

A LOW BACKGROUND-RATE DETECTOR FOR IONS IN THE 5 TO 50 keV ENERGY RANGE TO BE USED FOR RADIOISOTOPE DATING WITH A SMALL CYCLOTRON

Permalink

https://escholarship.org/uc/item/72t5060s

Author

Friedman, P.G.

Publication Date

1986-11-01

Lawrence Berkeley Laboratory
UNIVERSITY OF CALIFORNIA

Physics Division

MAR 2 1987

A LOW BACKGROUND-RATE DETECTOR FOR IONS IN
THE 5 TO 50 keV ENERGY RANGE TO BE USED FOR
RADIOISOTOPE DATING WITH A SMALL CYCLOTRON

P.G. Friedman
(Ph.D. Thesis)

November 1986

DISCLAIMER

A Low Background-Rate Detector for Ions in the 5 to 50 keV Energy Range to be used for Radioisotope Dating with a Small Cyclotron

Ph.D. Thesis in Physics

Peter Gray Friedman

University of California, Physics Department

and

Lawrence Berkeley Laboratory, Physics Division

University of California

Berkeley, CA 94720

25 November 1986

Table of Contents

Tables and Figures

Acknowledgments

I wish to thank the people who have traveled the road with me and who have made my journey more fruitful. Rich Muller, my thesis advisor, taught me that a physicist can travel many roads. He supported me and encouraged me to pursue my inspiration for this ion detector, and he gave me the opportunity to be eclectic in graduate school. Terry Mast lightened my load with insightful discussions and helped me to see the forest through the trees when I had lost my way. Luis Alvarez taught me to be sure of where I am headed and to report what I see clearly.

Maynard Michel generously loaned me the use of an entire lab, including the wonderful mass separator he built, while I assembled and tested the detector. More important, he gave me the benefit of his time, knowledge, and experience from which I learned daily. Saul Perlmutter traveled this road beside me from the beginning to the end. He is a good listener and a fine companion.

Ed Eberhardt answered countless questions about microchannel plates. Leonard Dietz provided critical information about secondary-electron emission.

My parents had faith in me and encouraged me to find my own way. My daughter Erica put up with seeing me less than she wanted and greeted me joyfully when I came home.

Most of all I thank Suzanne, for walking with me when the road is rocky.

A Low Background-Rate Detector for Ions in the 5 to 50 keV Energy Range to be Used for Radioisotope Dating with a Small Cyclotron

Peter Gray Friedman

Abstract

Accelerator mass spectrometry in tandem Van de Graaff accelerators has proven successful for radioisotope dating small samples. Small, inexpensive cyclotrons serving this purpose would make the technique accessible to more researchers and inexpensive enough to compare many small samples. To this end we are developing a 20 cm diameter 30 to 40 keV cyclotron dedicated to high-sensitivity radioisotope dating, initially for ^{14}C. At this energy, range and dE/dx methods of particle identification are impossible. Thus arises the difficult problem of reliably detecting 30 to 40 keV ^{14}C at 10^{-2} counts/sec in the high background environment of the cyclotron, where lower energy ions, electrons, and photons bombard the detector at much higher rates.

To meet this challenge we have developed and tested an inexpensive, generally useful ion detector that allows dark-count rates below 10^{-4} counts/sec and excellent background suppression. With the cyclotron tuned near the ^{13}CH background peak, to the frequency for ^{14}C, the detector suppresses the background to 6×10^{-4} counts/sec. For each ^{14}C ion the detector's grazing-incidence Al_2O_3 conversion dynode emits about 20 secondary electrons, which are independently multiplied in separate pores of a microchannel plate. The output signal is proportional to the number of secondary electrons, allowing pulse-height discrimination of background. We have successfully tested the detector with positive ^{12}C, ^{23}Na, ^{39}K, ^{41}K, ^{85}Rb, ^{87}Rb, and ^{133}Cs at 5 to 40 keV, and with 36 keV negative ^{12}C and ^{13}CH. It should detect ions and neutrals of all species, at energies above 5 keV, with good efficiency and excellent background discrimination. Counting efficiency and background discrimination improve with higher ion energy. The detector can be operated at least up to 2×10^{-7} Torr and be repeatedly exposed to air. The maximum rate is $10^{6.4}$ ions/sec in pulse counting mode and $10^{9.7}$ ions/sec in current integrating mode.

A Low Background-Rate Detector for Ions in the 5 to 50 keV Energy Range to be Used for Radioisotope Dating with a Small Cyclotron

> What seest thou else
> In the dark backward and abysm of time?
>
> Prospero, in Shakespeare's *The Tempest*

1. Introduction

The time each of us spends upon earth is but a fleeting instant. Indeed, the human race has inhabited the earth for a mere million years of its 4.5 billion year lifetime. For only the last few thousand years have we kept written records to tell future generations what has gone before them. Fortunately nature has provided us with means of probing the past to find our origins, both recent and cosmic. Radioisotopes are powerful tools for discovering temporal information about archaeology, evolution, climate, oceanography, geology, the history of the sun, the solar system, meteors, and cosmic rays.[1] The abundance ratio of an unstable isotope to a related isotope yields information about time scales that depend on the half-life of the unstable isotope. The relationship between the isotopes may be a chemical similarity, as for radiocarbon dating, or a shared decay chain, as for potassium-argon dating.

1.1. Accelerator mass spectrometry

The standard method for detecting many radioisotopes used for dating is decay counting. But the long half-lives that make these isotopes useful for dating old samples also make very small the fraction of such atoms that decay and can be counted in a reasonable time. Direct detection of the radioisotope by means of mass spectrometry is a much more efficient method, allowing both smaller samples and shorter counting times.

However, standard mass spectrometry cannot distinguish between trace levels of an isotope and background ions of similar mass. Even when it is possible to resolve nearby mass peaks of similar amplitude (in a histogram of the number of counts as a function of mass), the tail rejection is insufficient. That is, the tails of a mass peak are not steep enough to allow measurement of a trace-level isotope peak containing few counts near a background peak containing many counts.

In 1976, following work with Luis Alvarez on a quark search using the LBL 88" cyclotron as a mass spectrometer,[2] Richard Muller realized that one could use a cyclotron for direct detection of trace isotope abundances for dating.[3] Tests at the 88" cyclotron[4] showed that it was possible to reject backgrounds with mass differences of 1%, by a factor of 10^{-17}. However, when the cyclotron was tuned to accelerate ^{14}C, spurious background appeared, interfering with accurate carbon dating. This was apparently due to contamination of the cyclotron dees with ^{14}C from decades of use. Workers elsewhere have successfully used tandem Van de Graaff accelerators for carbon dating milligram size samples, a thousand times smaller than can be dated by decay counting.[5] Accelerators dedicated to dating overcome contamination problems. In January 1983 the NSF–University of Arizona tandem accelerator mass spectrometer facility[6] began dating real milligram carbon samples, as well as other isotopes, used in a large variety of research areas.

1.1.1. Radioisotope dating with a small cyclotron

As dating methodologies have become more sophisticated researchers have realized the benefit of dating many samples or many parts of a sample to reduce sources of systematic uncertainties such as contamination.[7] Accelerator mass spectrometry has made this possible by reducing the sample size required to obtain a date. This makes sample collection easier and allows one to date many things that could not previously be dated and

to date small parts of a sample individually. The technique has greatly increased the number of samples that it is technically feasible to date. However, the Arizona facility requires a large staff. This and the initial investment make such a facility costly, and there is a limited number of samples it can date each year. Also, bringing samples to a central facility is not as convenient as measuring them at a researcher's home institution, as was possible with decay counting.

In 1981 the LBL Astrophysics Group began developing a small cyclotron,[8] which we nicknamed the cyclotrino, to do radioisotope dating by accelerator mass spectrometry. The object is to make the technique more accessible, allowing more researchers to date more samples less expensively and more conveniently. We expect to achieve this with a small machine that is simple enough to be run by a single technician and inexpensive enough to be owned, for instance, by an archaeology department. We are initially developing the cyclotrino for carbon dating because, of the various isotopes useful for dating, the nearby background masses are most easily eliminated in the case of ^{14}C. After we understand how to use the cyclotrino for ^{14}C, minor modifications and different sources should allow the same machine to date samples using ^{10}Be and other isotopes.

To date a sample using ^{14}C one measures the abundance ratio of the unstable isotope ^{14}C to the stable isotope ^{12}C. This ratio is 1.2×10^{-12} in carbon that is in equilibrium with the biosphere. The ^{14}C is produced when cosmic ray collisions in the atmosphere liberate neutrons, which make ^{14}C in the reaction, $n + {}^{14}N \rightarrow {}^{14}C + p$. The ^{14}C reaches the rest of the biosphere in the form of $^{14}CO_2$. When a sample ceases exchanging carbon with the biosphere, the abundance ratio $^{14}C/^{12}C$ begins decreasing as the ^{14}C β-decays with a half-life of 5730 years.

The cyclotrino, shown in figure 1.1, functions as a many-pass mass spectrometer to
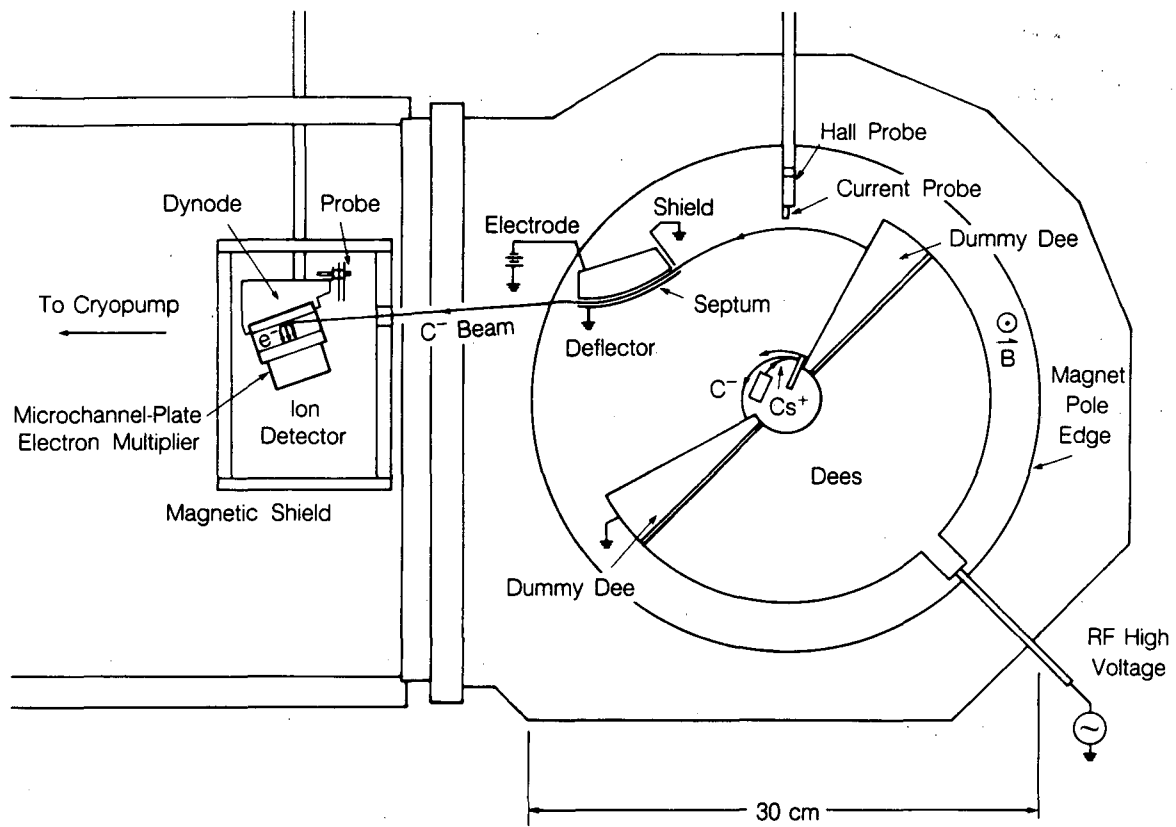
Figure 1.1   The detector is located close to the cyclotron dees in the presence of photons, electrons, and ions of energies up to a few keV. Quarter-inch thick cold-rolled steel shields the detector from the cyclotron's magnetic fringe field. We discuss the need for shielding in section 4.6.

detect the remaining ^{14}C directly. We tune it to accelerate ions of a particular mass by adjusting the frequency of the accelerating voltage between the cyclotron dees to match the cyclotron frequency for the corresponding charge-to-mass ratio. Ions with different masses fall out of phase with the radio-frequency accelerating voltage and are decelerated back to the center of the cyclotrino. Only ions with the correct mass are accelerated to the full 36 keV energy and pass through the curved electrostatic extractor without hitting the side.

The nearby backgrounds, which must be eliminated to measure ^{14}C, are ^{14}N, ^{13}CH, and $^{12}CH_2$. They differ from ^{14}C by $\Delta m/m$ of 1/83 000, 1/1800, and 1/1100 respectively.[9] Nitrogen has no stable negative ion so we eliminate it by accelerating negative ions in the cyclotrino. We require resolution sufficient to separate ^{14}C from ^{13}CH. The cyclotrino mass resolution is,[8]

$$R \equiv \frac{m}{\Delta m} = \frac{\nu}{\Delta \nu} \approx 2\pi H N \,,$$

where m is the mass, the radio frequency ν applied to the dees is about 15 MHz, the number of orbits N is about 30, and the harmonic H of the radio frequency with respect to the cyclotron frequency of the ion is about 15, so $R \approx 3 \times 10^3$. However, good enough resolution is necessary but not sufficient. The molecular backgrounds are more abundant than the ^{14}C by 8 to 11 orders of magnitude. Tail rejection of background masses is the crucial determinant of the cyclotrino's success.

Necessity being the mother of invention, we have used several innovations that are unusual in cyclotrons to achieve tail rejection in the cyclotrino. In addition to the low maximum energy and the acceleration of negative ions noted above, the source, injection, focusing, and detection of the ions are novel. The subsequent chapters describe the ion detector designed to meet the requirements detailed in the next section. In the present

internal cesium sputter source, a 3 keV Cs^+ beam bombards the solid carbon sample. It is believed that the cesium and carbon form a metastable neutral molecule. Because cesium has a low ionization potential, when the molecule dissociates, the carbon robs an electron from the cesium. A grid accelerates the resultant C^- to a 3 keV beam before it reaches the dee gap. In the near future[10] we will install a similar, off-the-shelf external source[11] to meet our need for easy sample changing and higher current. Figure 1.2 shows one possible configuration. In this source the Cs^+ beam hits a gas sample as it emerges from a porous tungsten plug producing about 10 to 100 μA of carbon current. This 5 keV beam will travel through a magnetic analyzer, after which Faraday cups scrape off the mass 12 and 13 amu constituents used to monitor the source current and calibrate the ^{12}C and ^{13}C abundances. The mass 14 constituents will be focused and possibly bunched to the optimum radio-frequency phase before the beam is injected radially into the cyclotrino. This requires bouncing the beam 180° off an electrostatic mirror[12] as shown in figure 1.2.

In the cyclotrino the beam is focused to the midplane of the dees using electrostatic focusing.[13] At high harmonic, this focusing is in fact due mostly to the reduction of fringe-field strength as the ions cross the gap between the dees. An ion is deflected toward the cyclotron midplane as it enters the fringe field and away—but less strongly—as it leaves. This is much simpler to analyze and construct than magnetic sector focusing, and it maintains the proper orbital phase unlike focusing that depends on a radially decreasing magnetic field. Electrostatic focusing strength typically decreases with radius. In the absence of magnetic focusing this overfocuses and blows up the beam at small radii. In the cyclotrino the ion is injected at a large enough radius to avoid this. Running at a high harmonic also reduces the focusing at lower radii because of averaging of the radio-frequency electric field, which changes sign several times while the ion is in the fringe field.
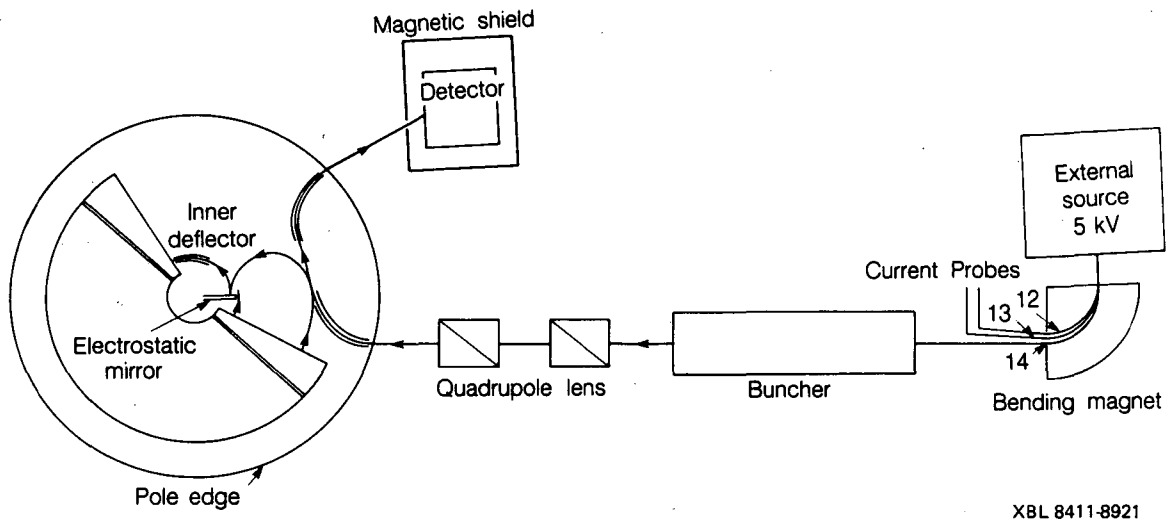
Figure 1.2   The figure shows a possible configuration for external beam injection as discussed in section 1.1.1.

Future generations of cyclotrinos may use permanent magnets and fit on a bench top. The size of the cyclotrino is now dominated by the approximately one cubic meter of space required by the yoke of the surplus NMR magnet we use to generate the field of about 10^4 gauss. The cyclotrino's low energy requires no radiation protection.

1.2. Ion-detection requirements

In general the advantage of dating with accelerator mass spectrometry over decay counting is sensitivity, rather than precision. Thus accelerator mass spectrometry is typically applied to problems where the small number of trace isotope atoms available to count is the limiting factor. In such samples however, background isotopes with similar masses are present at levels many orders of magnitude higher than the trace isotope level. Thus a detection system for accelerator mass spectrometry dating must be sensitive enough to efficiently detect the trace isotope, yet be insensitive to background ions. Previous accelerators used for dating have been operated in the 5 to 50 MeV energy range. These energies are high enough to allow range and dE/dx methods of particle identification to eliminate background ions. However, the range of a 36 keV ^{14}C from the cyclotrino is on the order of 100 to 1000 Å in aluminum,[14,15,16] so these methods are not currently possible.

In the case of the cyclotrino, low ^{14}C/^{12}C ratios in old samples and limited source current yield low count rates. The lower limit on count rate is set by two things. First, the magnetic field strength must remain constant to about one part in 10^4 for the duration of a measurement. The magnet is that stable for about 10^4 sec. Second, we want to make 10% or better measurements of the number of ^{14}C atoms. This requires counting more than 100 atoms in less than about 10^4 sec. Thus 10^{-2} counts/sec is minimum count rate we need to design for with the present system. Unlike in high-energy physics experiments, we can measure the background count rate with no beam present by detuning

the radio frequency. We then subtract this background rate from the total detector count rate to find the beam-ion count rate. In order to subtract the background reliably we want to keep the total detected background rate below 10^{-3} counts/sec.

The obvious source of background that the detector need suppress is ^{13}CH and $^{12}CH_2$ ions that are partially accelerated and then are scattered by residual gas molecules to reach the detector with less than about $2\,keV$. There is no direct path through the extractor. Reaching the detector with less than full energy would take a minimum of about four scatters. For any given ion this is less likely than an accidental four-bounce pool shot into the far corner pocket. However, since there is a factor of 10^8 to 10^{11} more ^{13}CH and $^{12}CH_2$ than ^{14}C, the detector must be able to distinguish between $36\,keV$ ^{14}C and the other ions which will reach it with less than $2\,keV$ energy. In addition, the cyclotrino produces electrons, UV, and soft x rays, some of which reach the detector, and electronics noise from high-voltage discharge and radio-frequency pickup. These too must be distinguished from $36\,keV$ ^{14}C ions.

Since the cyclotron selects for mass and the extractor selects for energy, the detector need only count the $36\,keV$ ions that reach it while discriminating low-energy background. It is not necessary that the detector discriminate between ions on the basis of mass or small differences in energy.

In addition to the need for background suppression, use in developing the cyclotron places other requirements on the detector. The detector must operate at 10^{-7} to 10^{-6} Torr and withstand frequent exposures to air. We also required that the detector fit in the existing cyclotron pressure vessel and through the air-lock probe (54×35 mm) of the mass spectrometer we used to test it.

1.2.1. Limitations of other detectors

None of the detectors commonly used to detect 5 to 50 keV ions meet these design requirements. Faraday cups cannot count individual ions. Detectors that use discrete-dynode electron multipliers require reactivation after exposure to air and their dark-count rate is too high. Adding a high-yield first-stage dynode for conversion of the ion to secondary electrons does allow discrimination of much dark noise and background. However, the lowest dark-noise rate achieved is still about 10^{-2} counts/sec.[17,18,19] In Daly, or doorknob, detectors[20,21] ions are postaccelerated so ions of widely varying energies generate the same size pulses. This makes background discrimination impossible. Channel electron multipliers and microchannel plates are often used as ion detectors. They may be exposed to air without requiring reactivation. However, they too produce an output signal for background ions, electrons, and photons that is the same size as that for higher energy ions. Solid state detectors have background and dark-noise rates that are too high even when cooled to liquid nitrogen temperature. Their small output pulses make them particularly susceptible to the electronic noise generated by a cyclotron. Also, the thinnest surface barrier (the metal electrode through which radiation enters the detector) available on state-of-the-art detectors is a few hundred Å, comparable to the range of a 36 keV carbon ion.

1.3. This detector

To meet the design requirements we have combined the background-discrimination capability of a high-yield conversion dynode with the air compatibility and narrow pulse-height distribution of a saturated microchannel-plate electron multiplier. The dynode preamplifies the ion signal before that signal, as well as unwanted dark noise and background, is amplified by the electron multiplier. This allows us to set a discrimination threshold to accept the large pulses from 36 keV ions while rejecting the smaller pulses from the various background sources. We expect this detector will be generally useful for

detecting ions above 5 keV in applications requiring low count rates or background suppression. The detector should also be useful in mass spectrometry because its response should be insensitive to beam position.

We have built the detector and tested it in a well-understood mass spectrometer both to calibrate it for use in the cyclotron and to explore its parameter space for more general use. To help other experimenters decide whether this design would be of use to them we tested as many parameters as possible. We tested it with positive and negative ions of various species, ^{12}C through ^{133}Cs, at 5 keV through 40 keV. As a rule, higher energies allow higher counting efficiencies and lower backgrounds. Finally we tested the detector in the cyclotrino and found that the background suppression surpassed the design goal.

2. Design

2.1. Theory of operation

The purpose of the detector design described below is to generate a large signal pulse in response to a full-energy ion while keeping the rate of large dark-noise and background pulses as low as possible. The detector uses a two-stage amplification scheme. In the first stage, the conversion dynode preamplifies the ion signal by emitting more secondary electrons when more energetic ions hit it. The dynode emits few secondary electrons in response to background ions, photons, and electrons. In the second stage the microchannel plate independently multiplies each secondary electron by about 10^7. The anode collects the total charge, which is proportional to the number of secondary electrons emitted by the dynode. The total charge arrives at the anode within the time constant of the amplifier and discrimination electronics so the ion signal is detected as a single large pulse.

There are two tricks that allow the detector to give proportional output. First, the holes, or pores, in the microchannel plate form a two-dimensional array of thousands of independent electron multipliers, each of which produces a fixed-size pulse when fired. Second, the dynode emits the electrons with a few eV of transverse energy. They move away from each other as they drift toward the microchannel plate and fire different pores.

In contrast to signal ions, dark noise and background usually cause no more than a single secondary electron to reach the microchannel plate and fire a single pore. Nonetheless, for reasons discussed in section 3.4.3, there is a low rate of background pulses above any given pulse-height threshold. The detector design attempts to achieve consistently large signal pulses in order to allow use of the highest possible discrimination threshold for any given beam-ion counting efficiency. A high threshold minimizes the rate of dark-noise and background pulses that will be counted.

2.2. Mechanical description of detector

The detector consists of two parallel plate electrodes, 35×47 mm, with a drift field in the gap between. One electrode holds the dynode and the other holds the microchannel plate. Figures 2.1 and 2.2 show the detector. The dynode (missing in figure 2.2) is dovetailed into a slot at the center of the dynode holder and may be easily replaced, as shown in figure 2.3. The 13×19 mm dynode (3 mm thick) is made of flat, polished aluminum. The dynode holder mechanically supports the rest of the detector by a 10 mm-thick glass-ceramic insulating standoff connected to the electron-multiplier holder. Directly opposite the dynode, the electron-multiplier holder has a similar-size hole through which secondary electrons approach the microchannel plate. Ten gold-coated 1 mil tungsten field wires span this hole and a sliding door covers the hole when the detector is out of vacuum to protect the microchannel plate from dust. Because the microchannel plate proved to be quite robust, the sliding door turned out to be an unnecessary complication. The detector is mounted on a cradle, so that its angle may be adjusted about an axis just behind and parallel to the dynode.

2.3. Microchannel-plate electron multiplier

A microchannel plate is a disk of high-resistivity semiconducting glass, pierced by many tiny pores, each of which is a continuous-dynode electron multiplier.[22,23,24,25] The remaining web of glass on each side of the disk is covered by a metal electrode used to apply a voltage. For our purposes, the important feature of a microchannel plate is its ability to independently multiply electrons incident on different pores. Although nearby pores are temporarily affected by having some of their stored charge robbed, the entire rest of the plate is available for simultaneous, independent multiplication of other incoming secondary electrons. The recovery time for fired pores is on the order of 50 to 100 msec (section 4.2).
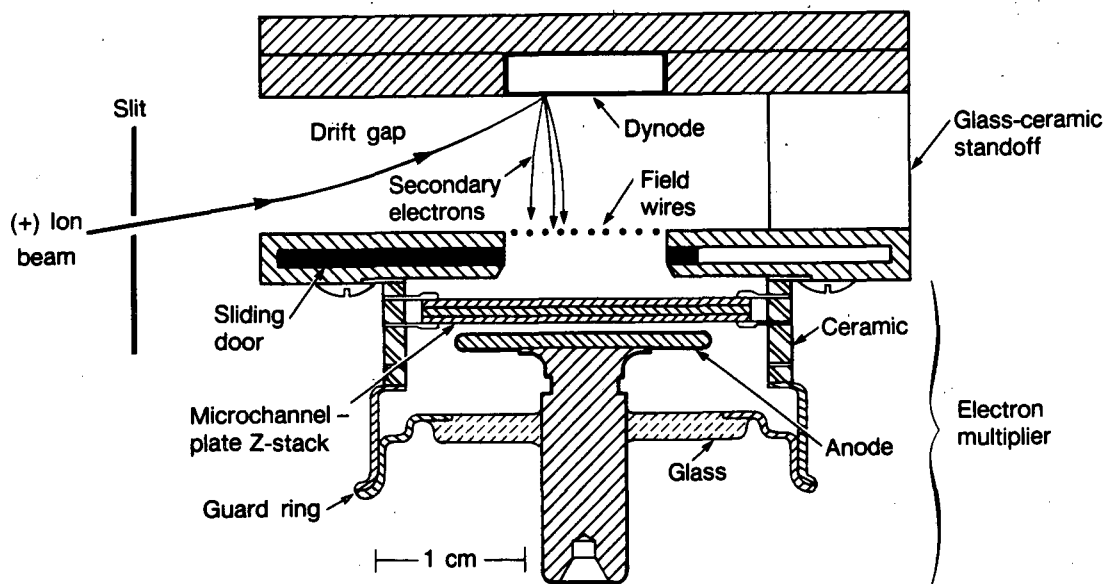
XBL 8610-11735

Figure 2.1 An ion beam (positive ions shown) hits the Al_2O_3 conversion dynode at grazing incidence. The ion ejects a few tens of secondary electrons with a few eV of transverse energy. The electrons move away from one another as they are accelerated through 1 kV across the 1 cm drift gap toward the microchannel-plate face. Each electron fires a separate microchannel-plate pore, which independently multiplies the electron and generates a pulse of $\sim 10^7$ electrons. The anode collects the total charge.
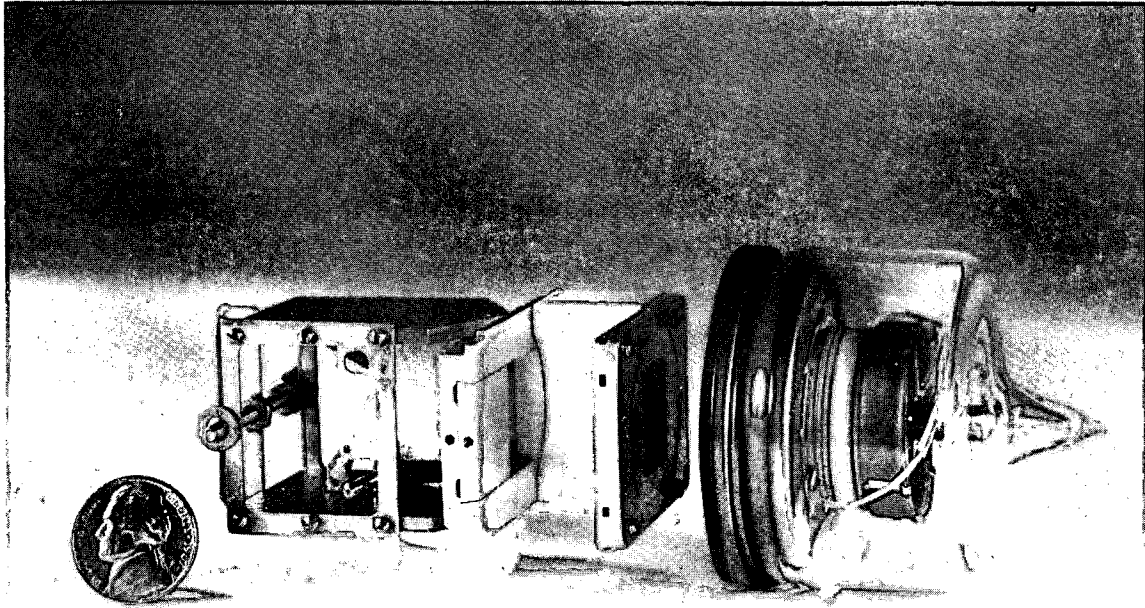
Figure 2.2.   This photograph of the detector shows the electron multiplier, in its proper orientation, before we unpacked it from the glass and metal vacuum vessel in which it was delivered. The replaceable dynode is removed. To the left of the dynode holder is the cradle used during tests in the mass spectrometer to adjust the orientation of the detector for different ion-incidence angles. A different mount was used to hold the detector in the cyclotrino.

We use an ITT F4129 Z-stack microchannel-plate open-window x-ray detector[26] (serial number 098104) for the electron multiplier. We chose this electron multiplier because it was relatively inexpensive ($1200 in 1982) since the manufacturer uses it in their F4129 microchannel-plate phototube.[27] It consists of three microchannel plates, an anode, and a guard ring in a ceramic and glass housing as shown in figure 2.1. The microchannel plates are stacked with no spaces between them and alternating 5° bias angles on the pores of each plate to prevent ion feedback (hence the name Z-stack). There are voltage leads for both ends of the microchannel-plate stack, the anode, and the guard ring. Typically, a pore fired in the input plate fires three adjacent pores in the middle plate and six or seven in the output plate. Each plate contains 1.3 million pores, 12.5 μ in diameter and 15 μ on center, within its 18 mm diameter active area. The upper limit on the number of independent electron multipliers is the total number of pores in one microchannel plate divided by the 6.5 pores typically fired in the output plate, or about 2×10^5. Eberhardt[26] provides an extensive list of values for various parameters of the F4129 multiplier.

We operate the electron multiplier in the pulse-counting mode, in which the voltage across the plates is high enough that the pulse height saturates, limiting the output charge.[22,24,27a] Saturation occurs in a pore when the number of electrons in an avalanche becomes large enough that it leaves a deficit of charge on the walls farther up the pore. This reduces the local electric field and thereby reduces the impact energy of electrons in the avalanche, which lowers the average gain per collision asymptotically to unity. Thus for a given voltage across the microchannel-plate stack the output is about the same size each time a pore is fired in the input plate.

The wall thickness between pores is 2.5 μ at its narrowest. This is a typical range for ions of a few MeV. Up to at least that energy, ions hitting the microchannel plate directly will fire only one pore in the input plate. Thus the background pulses they

generate will be about the same size as those from an incident electron.

2.4. Electronics

The detector requires that the dynode, the microchannel-plate input and output, and the anode be held at four different relative potentials spanning 3 or 4 kV. For convenience, these relative potentials may be floated with respect to ground. To allow independent adjustment of each potential during testing, we used three or four high-voltage supplies to run the detector. In typical use only one or two supplies and a voltage divider would be required. Figure 2.4 shows typical operating voltages. Each supply feeds voltage through a simple RC low-pass filter to remove ripple and noise. The 9 V battery between the field wires and the microchannel-plate input prevents secondary electrons emited at the field wires or electron-multiplier holder from reaching the microchannel plate. We were concerned that a single secondary electron from a background event could hit a field wire and eject more secondary electrons that could fire several pores in the microchannel plate. We later found that we need not have worried about this since the mean secondary-electron yield for an electron on gold reaches its maximum of only 1.46 at 750 V.[28] Nonetheless, the 9 V potential increase may prevent some background electrons from reaching the microchannel plates.

The output pulse of electrons from the microchannel-plate stack collects on the anode in a pulse with a FWHM of about half a nanosecond.[27] At typical gains used during testing, this negative signal pulse was too large for the standard charge sensitive preamplifiers we had available so we capacitively coupled the signal directly into a voltage amplifier. (In the cyclotrino we use a lower gain with a preamplifier.) From the amplifier we fed the signal into a pulse-height analyzer/multichannel scaler, a discriminator, rate meter, counter, and oscilloscope. To be compatible with the pulse-height analyzer the amplifier inverts and shapes the pulse with a full width at tenth maximum of about

Typical voltages

Dynode

Ion entrance slit   -1.0 kV

Field wires V_d

9 V Battery

Microchannel-
plate stack   0 kV

2.3 kV   } V_m

Anode

Guard ring   2.8 kV } V_a

Digital
Multimeter   2.8 kV

500 pF

100 nF

Amplifier

Oscilloscope   Discriminator   PHA/MCS

Rate meter   Timing counter
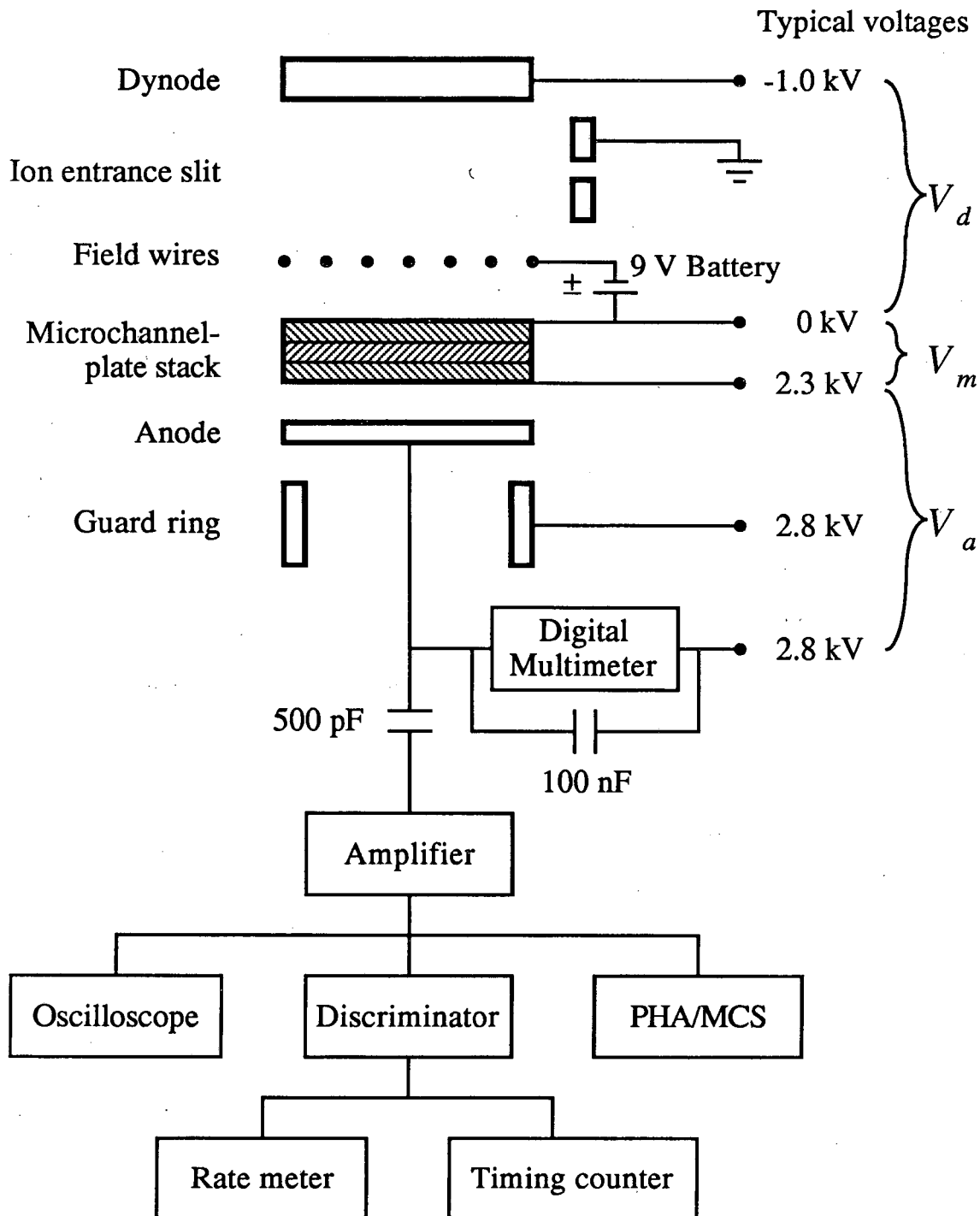
XBL 8610-11751

Figure 2.4   This diagram shows typical operating voltages and equipment that were used during testing.

1.5 μsec. We measure the electron multiplier's integrated output current by floating a digital hand-held multimeter on the anode high-voltage line. The meter has a calibrated 10 MΩ internal resister, so on the 10 V scale it reads current with a least count of 1 nA. A 100 nF capacitor across the meter's leads integrates current with a 1 sec time constant.

2.5. Ion-beam paths in drift gap

It is easy to calculate the first-order (parabolic) ion-beam paths within the detector by assuming a constant field within the drift gap and no fringe field. Unlike in a gravitational field, where all masses follow the same trajectory as long as they have the same initial velocity, in an electric field all masses (of similar charge) follow the same trajectory provided they have the same initial energy. Thus there is no need to readjust the angle of the detector when sweeping from one mass to another in either the cyclotrino or a conventional mass spectrometer. For the same reason, electrostatic lenses are used in mass spectrometry to allow sweeping through different masses without refocusing.

The curvature of the beam path causes the ion impact angle to be slightly different from the angle of the beam (with respect to the dynode) before it enters the drift gap. Positive ions curve toward the dynode and have a less grazing impact angle. For negative ions the opposite is true; neutral atoms travel in a straight line. For ion energies which are large compared to the 1 kV across the drift gap, this change in angle is small but still important because the secondary-electron yield is quite sensitive to angle near grazing incidence.

Because ion charge does affect the path of an ion in the drift gap, position of the detector with respect to the beam would have to be reset to center ion beams of different charge on the dynode. When switching between beams of different charge, one might also wish to reorient the angle of the detector with respect to the beam to keep the same ion

impact angle. This would maintain a more similar secondary-electron yield (section 3.3.1).

In addition to generating larger signals for ions with more energy, the detector has a limited ability to suppress any signal at all from ions of grossly different energy than the energy required for an ion to hit the center of the dynode. Because their paths curve differently in the drift field, these ions undershoot or overshoot the dynode, depending on whether they are positive or negative and have more or less energy than the ions to be counted (figure 2.5). This is particularly effective for collimated background particles with less energy than the beam. We calculate that for a 40 keV collimated beam aimed at the center of the dynode with an impact angle of 80°, positive ions entering the detector with an energy below about 10 keV in the same collimated beam would not reach the dynode for a drift-gap voltage of 1 kV. For ions that hit further than about 1 mm from the dynode, none of the secondary electrons can pass through the hole in the electron-multiplier holder to reach the microchannel-plate stack. Also, ions that miss the dynode create few, if any, secondary electrons because the surrounding aluminum is not polished (section 2.6).

In the cyclotrino the background has much lower energy than the beam ions but they are not well collimated. It is not clear to what extent the drift gap reduces the rate of small pulses from background ions. It should work well for background electrons.

2.6. Grazing-incidence conversion dynode

The function of the conversion dynode is to generate a signal, for each ion to be detected, that is large enough to be discriminated from the dark noise and background after each has been multiplied by the microchannel-plate electron multiplier. In order to get a large ion signal, we chose and configured the dynode to emit as many secondary electrons

$E > E_t$

$E = E_t$

$E < E_t$

Negative ion beam

$E < E_t$ $E = E_t$

$E > E_t$

Positive ion beam
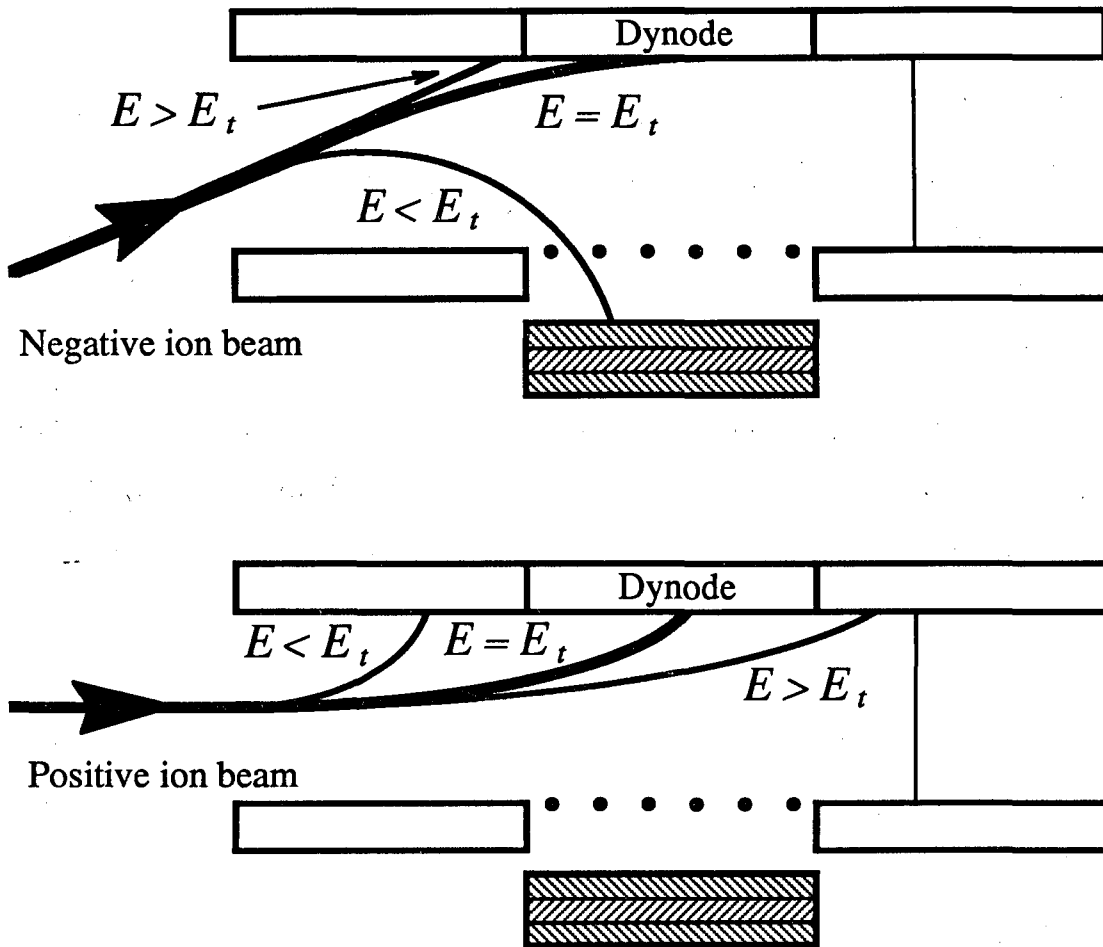
XBL 8610-11752

Figure 2.5   Background ions with lower or higher energy than E_t, the energy of the ions targeted on the center of the dynode, will miss the dynode and cause no pulse at all. This illustration (not to scale) indicates the paths of such ions. This low-energy background suppression is greatest for background ions that are well collimated with the beam. In the negative-ion case there is a small range of energies below E_t, for which the ions enter the microchannel plate directly. These ions fire a single pore causing a small pulse.

as possible for each beam ion, given the constraint of frequent exposure to air.

Dietz[29] suggested we use an aluminum oxide (Al_2O_3) dynode surface because it has a high secondary-electron yield, needs no activation, and is unaffected by to exposure to air.[30,31] The dynode will detect positive, negative, and neutral atoms and molecules. Negative ions have a slightly higher secondary-electron yield due to the presence of the additional electrons.[17] The yield of a molecular ion is typically comparable to the sum of the yields of its constituent atoms at the same velocity.[32] Following Dietz's early method,[19] we used 1100-0 aluminum (formerly designated 2S), which is specified to be 99.0% pure. We prepared the conversion surface by sanding with 600 grit sandpaper, and polishing in a magnesium-oxide powder and water slurry containing 2% nitric acid and 1% hydrofluoric acid. We found that aluminum-oxide powder, which Dietz used in his slurry, tended to scratch the surface because aluminum oxide is harder than aluminum. Magnesium oxide better matches the hardness of aluminum. We then allowed the surface to oxidize in air (for over a year, as it happened). Before assembling the detector we cleaned the dynode and other parts (except for the electron multiplier) in an ultrasonic cleaner, first with 1,1,1 trichloroethane, and then ethyl alcohol. On visual inspection the dynode we used is almost mirror smooth except for two barely discernible scratches and a very small pit.

We use the dynode at grazing incidence to take advantage of the secant dependence of secondary-electron yield on ion incidence angle from normal. This dependence arises because the secondary electrons have an escape depth of about 10 Å. The number which escape depends on the portion of the ion path length that remains within 10 Å of the surface. Various authors have seen the approximate secant dependence experimentally.[33]

Previous experimental data[32] have shown that surfaces emit secondary electrons with

a solid-angle density distribution approximately proportional to the cosine of the angle from normal. The typical energy distribution of emitted secondary electrons has a peak at between 0 and 2 eV, and a median below 5 eV.[32,34] The position of the mean and the length of the tail both decrease with increasing atomic number for incident alkali metal ions, Li, Na, K, Rb, and Cs. We were not able to find similar information for other columns of the periodic table. The energy distribution is insensitive both to the nature of the target and to ion energy up to several tens of keV.[35]

2.7. Detection of secondary electrons at microchannel-plate face

2.7.1. Separation between secondary electrons

It is critical that the detector's output pulse height be proportional to the number of electrons incident on the front face of the microchannel plate. This allows discrimination between full-energy ion signals, for which tens of electrons from the dynode hit the microchannel plate, and dark noise or background, for which few electrons hit the microchannel plate. Since we operate the electron multiplier in the saturated, pulse-counting mode, the output of a given pore is independent of how many electrons fire that pore simultaneously. Therefore the secondary electrons must land in well-separated pores for the electron multiplier to have the linear amplification required for a proportional output. This ensures that they are independently multiplied and that the output pulse height, which equals the sum of the outputs of the fired pores, is proportional to the number of incident electrons.

An electron incident on the front face of the Z-stack fires a group of seven pores in the output plate. As a result, a minimum separation of three pores between adjacent incident electrons is required. In practice a larger (but unknown) separation is required to ensure that each pore saturates completely since pores conductively borrow charge from their neighbors.

For a group of secondary electrons ejected by an ion impact at the dynode, we wish to derive the average separation D between adjacent electrons as they hit the microchannel plate. Consider N secondary electrons emitted with initial energy E_o, in a cosine angular distribution (section 2.6). In the center-of-mass frame of the electrons (which accelerates through the drift gap) they move away from one another in a small expanding hemisphere with a radius that remains much smaller than the drift gap. When the electrons reach the microchannel-plate face the hemisphere is projected into a disc. A secant factor arises from the projection, which cancels the cosine angular distribution, so the electrons are distributed uniformly over a disc on the microchannel-plate face. The product of the time of flight and the magnitude of the initial velocity gives the radius r of the disc.

$$r = (2s+s') \sqrt{\frac{E_o}{eV_d}} \ ,$$

where s is the distance (10.0 mm) from the dynode to the field wires, s' is the distance (6.0 mm) from the field wires to the microchannel-plate front face, e is the magnitude of the electron charge, V_d is the voltage increase (1 kV) from the dynode to the field wires. On average each of the N electrons owns the area contained in a disc of radius $R = r/N^{1/2}$. The average separation D between adjacent electrons is $2R$.

$$D = 2(2s+s') \sqrt{\frac{E_o}{eNV_d}}$$

As a worst case, consider 30 secondary electrons emitted from the dynode with only 1 eV. (We found that 20 to 30 secondary electrons was a typical range, section 3.3.1.) The electrons hit the microchannel-plate face within a disc of radius 830 μ, and the average distance between adjacent electrons is 300 μ, or a separation of 20 pores, 15 μ on center. This is large compared to the lower-limit separation of three pores. The separation increases as the square root of the initial energy of the electrons, so for the typical energy distribution the average separation is larger than 20 pores. We expect that an average

separation of 20 pores should be sufficient to ensure that the pulse size will not be reduced due to nearby pores firing. However, one needs to consider this separation before increasing V_d or decreasing the size of the drift gap substantially. We did not test to see that the multiplication was indeed proportional, but nothing in our data indicated that it was not.

Although we need the secondary electrons to separate sufficiently to be independently multiplied, too much separation will cause some of the secondary electrons to miss the hole in the electron-multiplier holder and not reach the microchannel plate. We calculate that less than about 25% of the secondary electrons will be lost for an ion hitting the dynode more than 1 mm from any edge.

2.7.2. Collection efficiency

The collection efficiency is defined as the probability that an electron that hits the microchannel plate will fire a pore and be multiplied. For the F4129 electron multiplier we are using, the manufacturer claims that the collection efficiency for electrons with greater than 200 eV is between 60% and 100% and quotes 85% as the nominal collection efficiency.[36] Measurements on other microchannel plates yield collection efficiencies of about 90%, even for electron energies as low as 100 eV.[37] On scales of 10 μ to 1 mm, the collection efficiency varies less than 1% (consistent with statistical fluctuations in the measurement) over the area of the microchannel plate.[38,39] There are variations of 5% to 10% over scales larger than 5 mm.[40]

3. Performance

3.1. Introduction to detector tests and results

In this chapter we first discuss the characteristics of the electron multiplier, which determine certain overall characteristics of the detector. We describe the detector's response to a single secondary electron from the dynode. Next we look at the detector response to ions of various species and energies and to background and dark noise. Most important, we compare the pulse-height distribution of the ion signal to the distributions of the background and dark-noise, and discuss the effect of discrimination on ion-counting efficiency and background-count rate in order to evaluate the overall performance of the detector in terms of dark-noise or background rate as a function of counting efficiency. We end the chapter by discussing the effects of exposing the detector to air and high currents, and of damage to the electron multiplier from high-voltage discharge.

We tested the detector in Maynard Michel's mass separator, a single-direction focusing mass spectrometer with a 1.5 m radius, 90° magnetic-sector analyzer. To enter the detector the beam had to pass through a 0.8×13 mm slit in a mask 5 mm in front of the detector. A micrometer-driven mechanical feedthrough allowed us to move the slit in the 0.8 mm direction. We used an oven-type $^{23}Na^+$ ion source. The unpurified sodium in the source also provided us with isotopes of the heavier alkali metals. In addition, charge-exchange collisions with stray hydrocarbon gas at the mouth of the source provided $^{12}C^+$. Unless otherwise stated, all results presented are from tests in the mass spectrometer.

Following the mass-spectrometer tests we successfully tested and used the detector in the cyclotrino. We obtained few quantitative results about the detector itself in the cyclotrino. However, with almost no effort to optimize the detector's performance in the cyclotrino, we achieved the design objective of detecting 36 keV $^{14}C^-$ ions at $(50 \pm 10)\%$

efficiency with a total background rate of 6×10^{-4} counts/sec. The ions not counted have pulse heights below the discriminator threshold. There is a small additional collection-efficiency loss because the beam extends beyond the dynode. We measured the typical background rate, 6×10^{-4} counts/sec, to about 10% but we saw fluctuations as large as 50% between runs on different days. The detector had been turned off between these runs. To the present it has been unnecessary to find the cause of these fluctuations since the background-level is low enough and stable enough within each run of several hours.

Table 3.1 shows the various epochs of data discussed throughout the text and the exposures to air between them. We give more details in relevant sections, especially section 3.6.1.

Table 3.1

Exposure of multiplier to air or dry N_2	Test apparatus	Ion incidence angle	Results
Multiplier attached to detector and inserted into mass spectrometer in dry N_2; no exposure to air.			
	mass spectrometer	80.0°	some useful results
Up to air for 18 minutes.			
	mass spectrometer	80.0°	no useful data
Up to air for 10 minutes.			
	mass spectrometer	82.3°	controlled tests, quantitative results
Up to air for ≈1 month.			
	cyclotrino	≈75°	few quantitative results on detector
Up to air 6 to 12 times for > several hours each during use in cyclotrino.			

3.2. Pulse-height distribution from multiplication of a single secondary electron

The detector generates a signal for each ion that hits the dynode. The pulse-height distribution of these signals we call the ion distribution. The ion distribution is the convolution of the distribution of secondary-electrons ejected by ions hitting the dynode, with the pulse-height distribution for multiplication of a single secondary electron by the electron multiplier. This latter pulse-height distribution we call the single-electron distribution. We measured the single-electron distribution to study both the signal and the background of the detector. Most of the background pulses result from a single secondary electron multiplied by the electron multiplier, so we expect the background distribution to be similar to the single-electron distribution. Knowing the secondary-electron distribution also allows us to study the microchannel-plate gain and relative collection efficiency as functions of incident secondary-electron energy (section 3.2.1) and the absolute gain as a function of the voltage across the microchannel-plate stack, V_m (section 3.2.2).

To measure the single-electron distribution, we illuminated the dynode with UV photons from a mercury-vapor lamp through a window in the mass spectrometer. This yielded a low rate (less than 10^3 counts/sec) of photoelectrons, which fired the microchannel plate one electron at a time. We varied the energy with which the electrons hit the microchannel plate by varying the voltage increase V_d from the dynode to the microchannel-plate front face. It was not possible to illuminate only the dynode. Instead some photons hit the microchannel plate directly and generated pulses. Thus the raw pulse-height distributions for these data include pulses generated by photoelectrons emitted from both the dynode and the microchannel plate.

The upper curve in figure 3.1(a) shows the raw distribution for $V_d = 1.0\,\mathrm{kV}$. We also measured the pulse-height distribution of pulses from photons hitting only the microchannel plate, by back-biasing the dynode (negative V_d) so no electrons from the
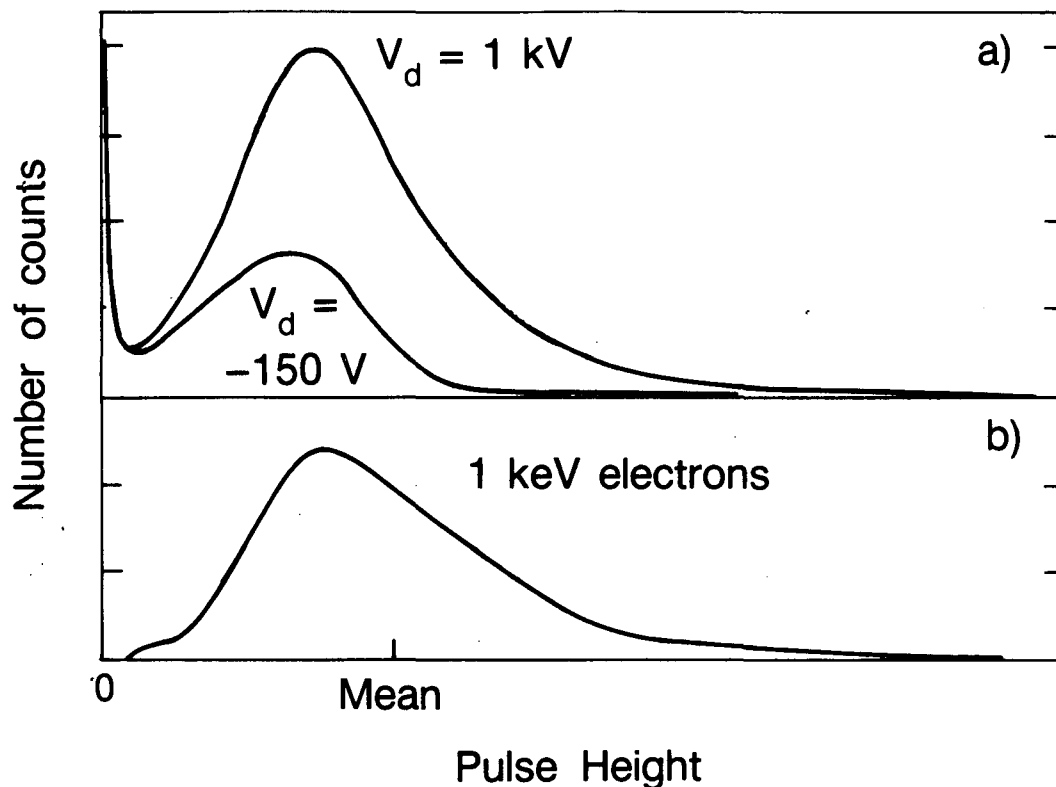
Figure 3.1   Three pulse-height distributions for single photoelectrons are shown. The curves are tracings through pulse-height analyzer photographs. Typical errors are a few percent. The three curves are for data taken with $V_m = 2.3\,\mathrm{kV}$. Figure 3.1(a) shows the raw distributions of pulses from photons that hit both dynode and the microchannel-plate face (upper curve), and from photons that hit only the microchannel-plate face (lower curve). Figure 3.1(b) shows the difference of the raw distributions, which is the single-electron distribution for 1 keV electrons from the dynode. The mean of the distribution is $5.14 \pm 0.10\,\mathrm{pC}$, indicating that the electron-multiplier gain is $3.21 \times 10^7\,e^-/e^- \pm 1.9\%$.

dynode could reach the microchannel plate. The distribution of pulses from photons hitting only the microchannel plate (the lower curve in figure 3.1(a)) should be completely insensitive to changes in V_d because the microchannel plate is shielded from the field in the drift gap by the field wires shown in figure 2.1. We subtracted this distribution from the raw distribution. The resulting single-electron distribution, figure 3.1(b), is the detector response to electrons emitted at the dynode and should be valid for each of the secondary electrons ejected by an ion hitting the dynode.

For the single-electron distribution of 1 keV secondary electrons shown in figure 3.1(b), the FWHM is $(85 \pm 5)\%$ of the mean, or $(106 \pm 6)\%$ of the position of the peak. The manufacturer gives the nominal FWHM as $\approx 100\%$ of the position of the peak for the F4129 electron multiplier at $V_m = 2.4$ kV.[26] The distribution narrows as V_m increases, pushing the pulses further into saturation. Other references for Z-stack electron multipliers give values for the FWHM as low as 26% of the mean.[39] A lower FWHM indicates more effective saturation which might provide a steeper background-distribution tail, which would be better for our purposes. Below $V_m \approx 1.6$ kV, pulses in this electron multiplier do not saturate and the multiplier operates in the current mode. The resulting pulse-height distribution is monotonically decreasing with no peak.

3.2.1. Gain and collection efficiency as a function of incident-electron energy

Using the UV source we also studied the effect of incident-electron energy on gain and collection efficiency, by varying V_d. To find the gain, which equals the charge per pulse, we divided the net integrated anode current by the net count rate, as measured by a pulse-height analyzer. The net count rate and current are the values for electrons emitted only at the dynode, corrected as above. We could not directly measure the absolute collection efficiency because we had no way to measure the number of secondary electrons leaving the dynode toward the microchannel plate. We did find the relative collection

efficiency as a function of incident-electron energy by measuring count rate versus V_d. We relied on the assumption that the UV source provided constant illumination. The count rate at $V_d = 100$ V was the same, to well within the statistical uncertainty, at the beginning and end of this series of measurements. This indicates that the illumination was constant.

Figure 3.2 compares these data with the manufacturer's data[41] for an electron multiplier with a similar kind of plate (a single "C-plate" containing curved pores with an 80:1 aspect ratio). The manufacturer's data are normalized to these data at 500 eV. The gain on the C-plate was probably about 10^7. The two sets of data are similar. This implies that the gain and collection efficiency depend on surface characteristics that are similar for the two plates. The gain and collection-efficiency curves reach apparent plateaus for V_d above about 500 V. We prefer that the collection efficiency be as close to 100% as possible so that each signal pulse will be as large as possible. The plateau is necessary but not sufficient to ensure collection efficiency near 100% at higher voltages.

Figure 3.2 shows that the mean pulse height of 1 keV electron pulses is larger than those from electrons with nearly zero energy by $(48 \pm 5)\%$. We believe the reason for this increase of gain with electron energy is the following. Electrons with close to zero energy can fire no more than one pore in the first microchannel plate. However, when a 1 keV electron from the dynode hits the microchannel-plate face it can eject more than one secondary electron, which fire more than one pore. This hypothesis is supported by the increase in the length of the tail of the single-electron distribution with increasing energy of secondary electrons. One can see this by comparing the lower curve in figure 3.1(a), for photoelectrons ejected from the microchannel-plate face with less than 5 eV, and the 1.0 keV curve in figure 3.1(b). Contrary to what one might expect there is not a second, two electron, peak in figure 3.1(b). This may be because the fired pores are near enough to one other so their avalanches overlap in the second and third plates in the stack. Thus
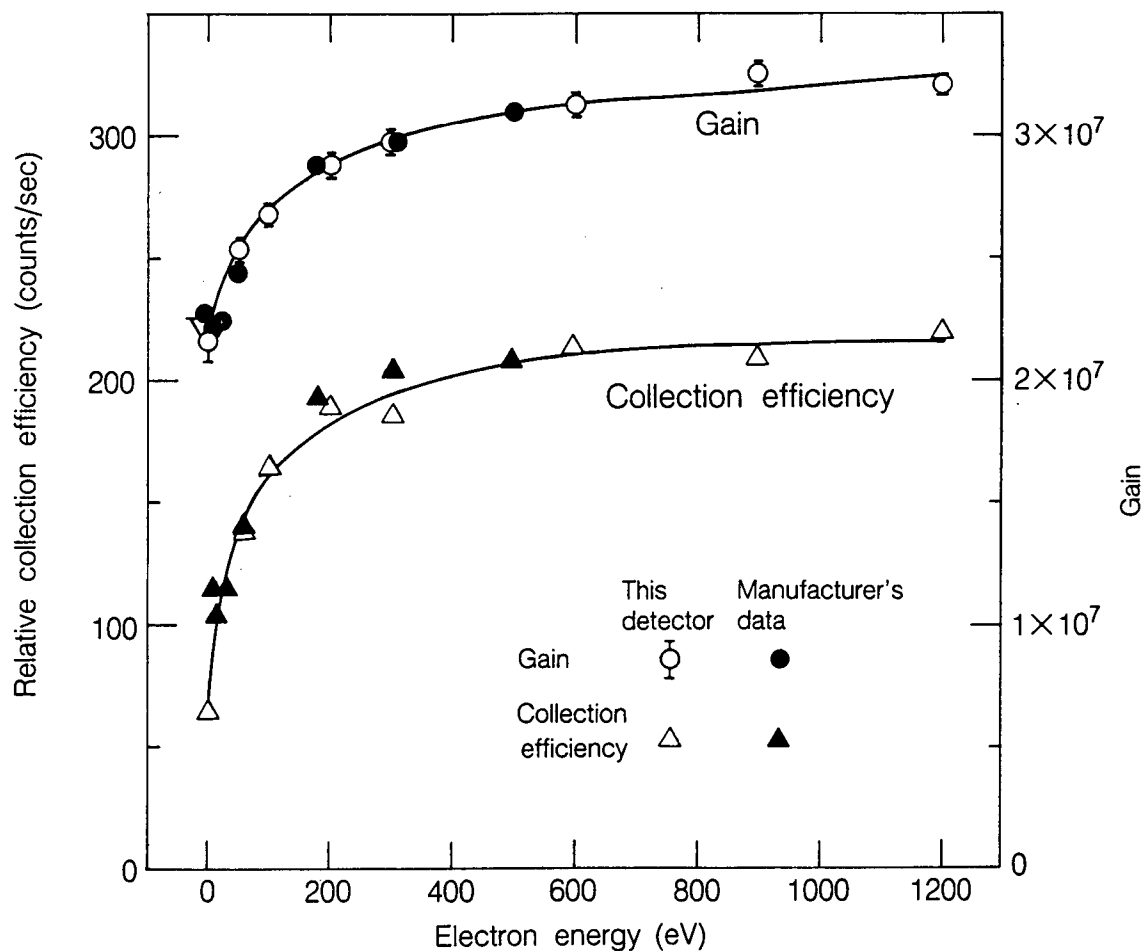
Figure 3.2   The microchannel-plate gain and collection efficiency are shown as a function of incident electron energy. The manufacturer's data[41] for both gain and collection efficiency have been normalized at 500 V to the data for this detector using hand-drawn curves through the detector data.

the total charge output varies depending on the distance between the fired pores, smearing out the distribution.

3.2.2. Gain as a function of microchannel-plate voltage

We want to know the absolute microchannel-plate gain as a function of V_m for several reasons. In pulse-counting mode $(V_m > 1.6\,\text{kV})$ we require it to calibrate the ion pulse-height distribution in terms of secondary electrons emitted from the dynode. Similarly in current mode $(V_m < 1.6\,\text{kV})$ we use it to determine the ion current from the measured anode current. It also allows us to calculate the maximum allowable ion count rate at different gains (section 4.1).

We measured the gain directly, using single photoelectrons as described above, at $V_m = 2.3\,\text{kV}$ and $V_m = 2.5\,\text{kV}$. At other values of V_m we derived the gain from data on the mean pulse height for 40 keV Cs or K ions (section 3.3). To do so we assumed that the ratio of the output charge per ion pulse to the output charge per single electron pulse remains constant at all V_m for a given ion. This ratio is the mean number, per ion, of secondary electrons collected at the microchannel-plate face. This equals the dynode secondary-electron yield times the collection efficiency. The dynode yield is independent of V_m. However, the collection efficiency may decrease with V_m because it may depend on the attractive electric-field strength at the entrance to the pores, which is proportional to V_m. This would change the ratio at lower V_m but the effect would probably be negligible in determining the gain from ion data since the gain varies steeply with V_m.

We made most of the quantitative measurements presented in this work after the electron multiplier's second exposure to air, with an ion incidence angle of 82.3°. Under these conditions, with $V_d = 1.0\,\text{kV}$, we measured the ratio of secondary electrons collected per Cs$^+$ at both $V_m = 2.3\,\text{kV}$ and $V_m = 2.5\,\text{kV}$. The measured ratios were

23.9 ± 0.4 and 23.8 ± 1.0 respectively. These results agree to within the uncertainty and give no indication of substantial collection-efficiency dependence on V_m. However, such a dependence might be stronger at lower V_m since the collection efficiency must go to zero at $V_m = 0$.

For both photoelectron and ion methods, we found the mean charge per pulse that reached the anode, by dividing the count rate (as measured by the pulse-height analyzer) into the current. For the photoelectron method the gain is the charge per pulse divided by the electronic charge. The ion method requires a further division by the number of secondary electrons collected per ion. After the second exposure to air, with $V_m = 2.3\,\text{kV}$ and $V_d = 1.0\,\text{kV}$, we measured the mean of the single-electron distribution to be $5.14 \pm 0.10\,\text{pC}$, equivalent to a gain of 3.21×10^7.

In order to explore the upper end of the detector's dynamic range for ion counting (section 4.1), we made measurements in the range $V_m < 1.6\,\text{kV}$, where the electron multiplier operates in current mode. Since pulse-counting is not feasible in this range, we used a variation of the ion method described above. We measured the anode current at different V_m, in overlapping regions below 1.6 kV, by alternately adjusting V_m at constant ion beam current, and ion beam current at constant V_m. We normalized these data to one another and to the pulse-count data at $V_m = 1.6\,\text{kV}$ to find the absolute gain at each V_m. Following these tests the gain at $V_m = 2.3\,\text{kV}$ dropped temporarily by 59% (section 3.6).

Figure 3.3 compares gain versus V_m curves for these data with data for three other F4129 Z-stacks. Lo and Leskovar[27] tested one of them. The manufacturer[41] tested the other two stacks before and after processing them with an "electron scrub" in preparation for installing them in phototubes. This process makes the gain more uniform over the
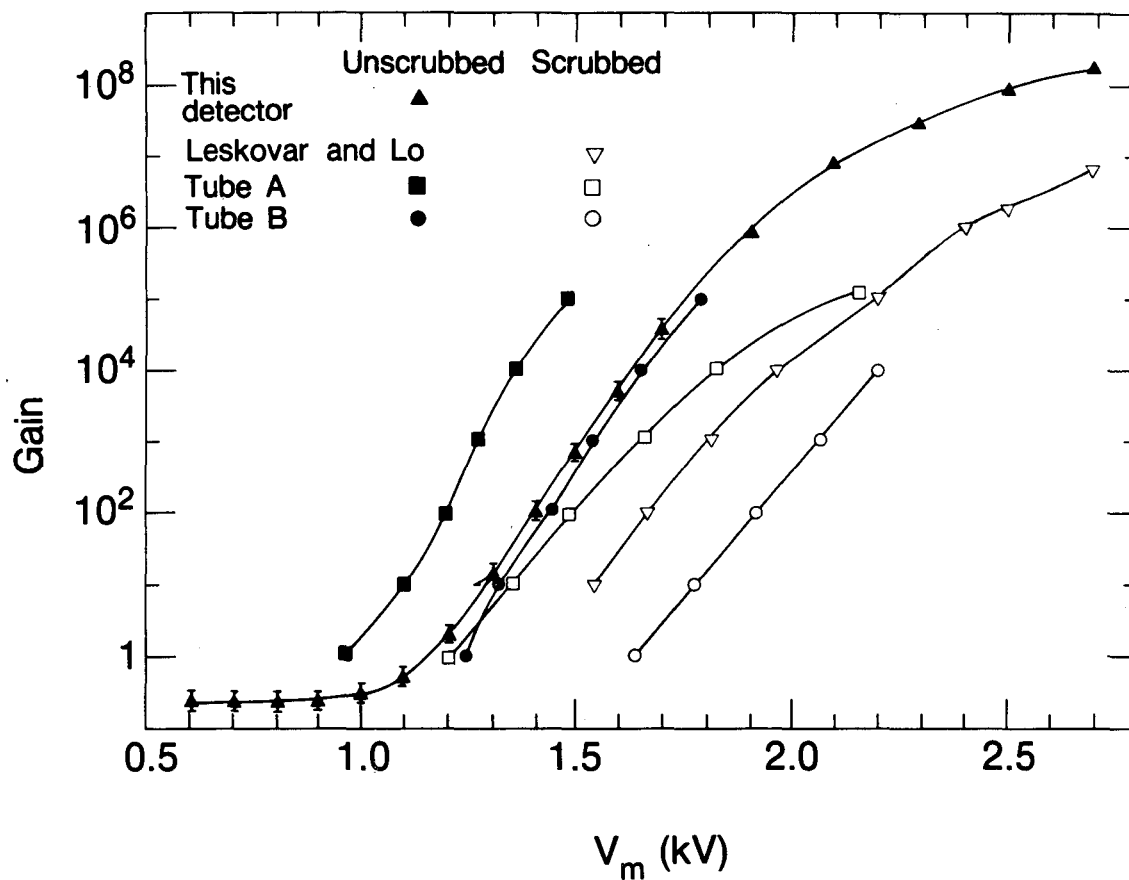
Figure 3.3   These plots of gain as a function of microchannel-plate voltage show the effect of electron scrubbing. The manufacturer's data for tubes A and B, and the highest data point of the Lo and Leskovar data, are unpublished.

microchannel-plate surface and more stable over time and use.[42,43] It also increases the V_m at which a given gain is reached as shown by the before and after curves for those two stacks. Given this increase, the high gain reached by this unscrubbed stack is consistent with Lo and Leskovar's data. The larger error bars on our data below 1.6 kV result from systematic uncertainties such as instability of the ion source and hysteresis of the microchannel-plate gain following large changes in input current. We do not understand the decrease of the slope to zero below 1.1 kV. Eberhardt[44,45] gives a power-law model for gain as a function of V_m for the lower part of the curve where the pulses do not saturate. For V_m between 1.2 kV and 1.7 kV we find an exponential gain increase to be a better fit. However, the difference is on the order of the uncertainty in the data.

3.3. Ion-signal pulse-height distribution

In this section we discuss the pulse-height distribution of the detector output (in the pulse-counting mode) in response to ions of various incidence angles, species, and energies. This ion distribution should depend to first order on only these parameters (and on dynode properties), which determine the dynode's secondary-electron yield distribution, not on the detector voltages, which determine the much narrower single-electron distribution. In section 3.3.1 we show that this is indeed the case and that the dependences on these parameters agree with those quoted in the literature. In subsequent sections we compare the ion-signal distributions to those of dark noise and background. We took the data discussed in this section with $V_m = 2.3$ kV (except as noted below), $V_d = 1$ kV, and the voltage increase from the output end of the microchannel plate to the anode, $V_a = 500$ V.

Section 3.2.2 describes how we found the pulse-height scale, in secondary electrons, that we use to describe the ion distributions. As is always the case in measuring secondary-electron yield distributions, we actually measure the number of secondary

electrons that are collected by the electron multiplier, not the larger number emitted by the dynode. We do not correct for the unknown collection efficiency. The results are valid for the actual collection efficiency of the electron multiplier. However, if the collection efficiency can be improved this would improve the detector performance by increasing the pulse-height of the ion distributions to a region of lower background. The single-electron distribution is too wide to resolve the individual peaks (at integer numbers of secondary electrons) that make up the ion distribution. This leaves a systematic uncertainty in the overall pulse-height scale due to uncertainty in the absolute gain of the microchannel plate for 1 keV secondary electrons. This gain uncertainty is 2% or 3% for most of the ion distribution data, which we took after the second exposure to air with an ion incidence angle of 82.3°. Due to systematic errors in early measurements, the uncertainty is about $^{+5}_{-10}$% for data taken at an 80.0°, before the first exposure to air (section 3.6).

The mean pulse height of ion distributions drifted by ±1% (5% in one case) between tens of identical runs taken a few hours to a few weeks apart. This is greater than the statistical uncertainty of 0.3% in measuring the mean. This drift does not result from error in measuring the gain at a given V_m. That would merely cause an overall scale error for all of the ion pulse-height distributions measured in a period between exposures to air (table 3.1 and section 3.6). It would not introduce discrepancies between measurements taken at the same incidence angle, 80.0° or 82.3°. However, the drift could be caused by an actual gain change between runs, perhaps due to a change in V_m. From figure 3.3 one can derive that at $V_m = 2.3$ kV, the gain would drift by 1% for a 1.7 V drift in V_m. In addition, amplifier gain drift, poor electrical contacts in transmission cables, and changes in beam position or gas adsorption on the dynode could also be to blame for the drift in the mean of the ion distributions.

In the mass spectrometer we tested the detector with positive ion beams of ^{12}C, ^{23}Na,

^{39}K, ^{41}K, ^{85}Rb, ^{87}Rb, and ^{133}Cs at energies between 5 and 40 keV. Figure 3.4 shows ion distributions representative of the range of measured distributions. These data were taken at different times and rates, so they include different amounts of background. They are consistent with nearly 100% ion-counting efficiency for a discrimination threshold near zero. The wide valley between the background and the signal is important for effective background discrimination.

3.3.1. Effects of ion species, incidence angle, and energy on secondary-electron yield

The distributions for the lighter ions in figures 3.4(a) and 3.4(b) are wider and more skewed, with longer tails toward larger pulse heights. Dietz[30] also saw this effect and explained it in terms of electron-multiplication statistics. Quantitatively the details of the secondary-electron emission and angular scattering of the ions in the Al_2O_3 dynode determine the yield distribution. Qualitatively the secant dependence of secondary-electron yield on ion incidence angle explains the differences in the distributions for ions of different masses. For grazing incidence ions this dependence maps a distribution over ion angle into a secondary-electron yield distribution that is skewed toward larger pulse heights, as shown in figure 3.5. The angular distribution of ion paths, with respect to the dynode surface, is due to ion beam emittance, surface irregularity, and small angle scattering in the dynode. Since beam emittance and surface irregularity should be similar for all ions, this implies that ions with wider, more skewed distributions have larger angular scatter. Figure 3.5 also indicates that this effect should be more pronounced at larger mean incidence angles. In the measured distributions, figures 3.4(a) and 3.4(b), the tail lengths are indeed in order of ion mass and the effect is much stronger at 82.3° than at 80.0°.

We measured the effect of ion incidence angle, species, and velocity on mean secondary-electron yield. To find the mean yield we divided the integrated output current
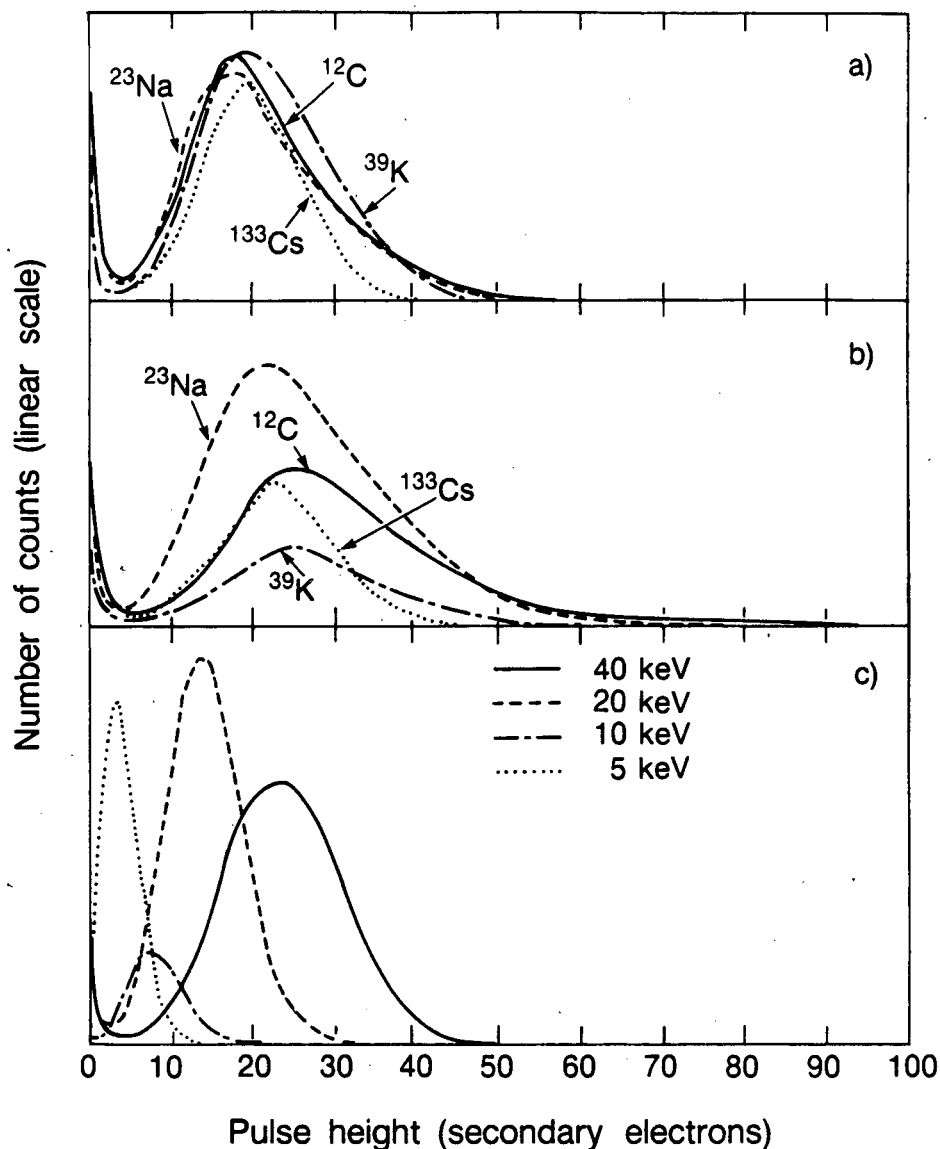
XBL 8610-11738

Figure 3.4   Pulse-height distributions are shown for (a) 40 keV ions at 80.0°, (b) 40 keV ions at 82.3°, and (c) $^{133}Cs^+$ ions at a nominal incidence angle of 82.3°. For (c) the calculated, actual incidence angles are 73.7°, 77.8°, 80.5°, and 82.3° for 5, 10, 20, and 40 keV respectively. The smaller pulse heights at lower energies are partly due to the smaller actual incidence angles. Figure 3.8 shows the corrected mean yield as a function of energy alone. All distributions are for positive ions and all curves are tracings from pulse-height analyzer photographs.
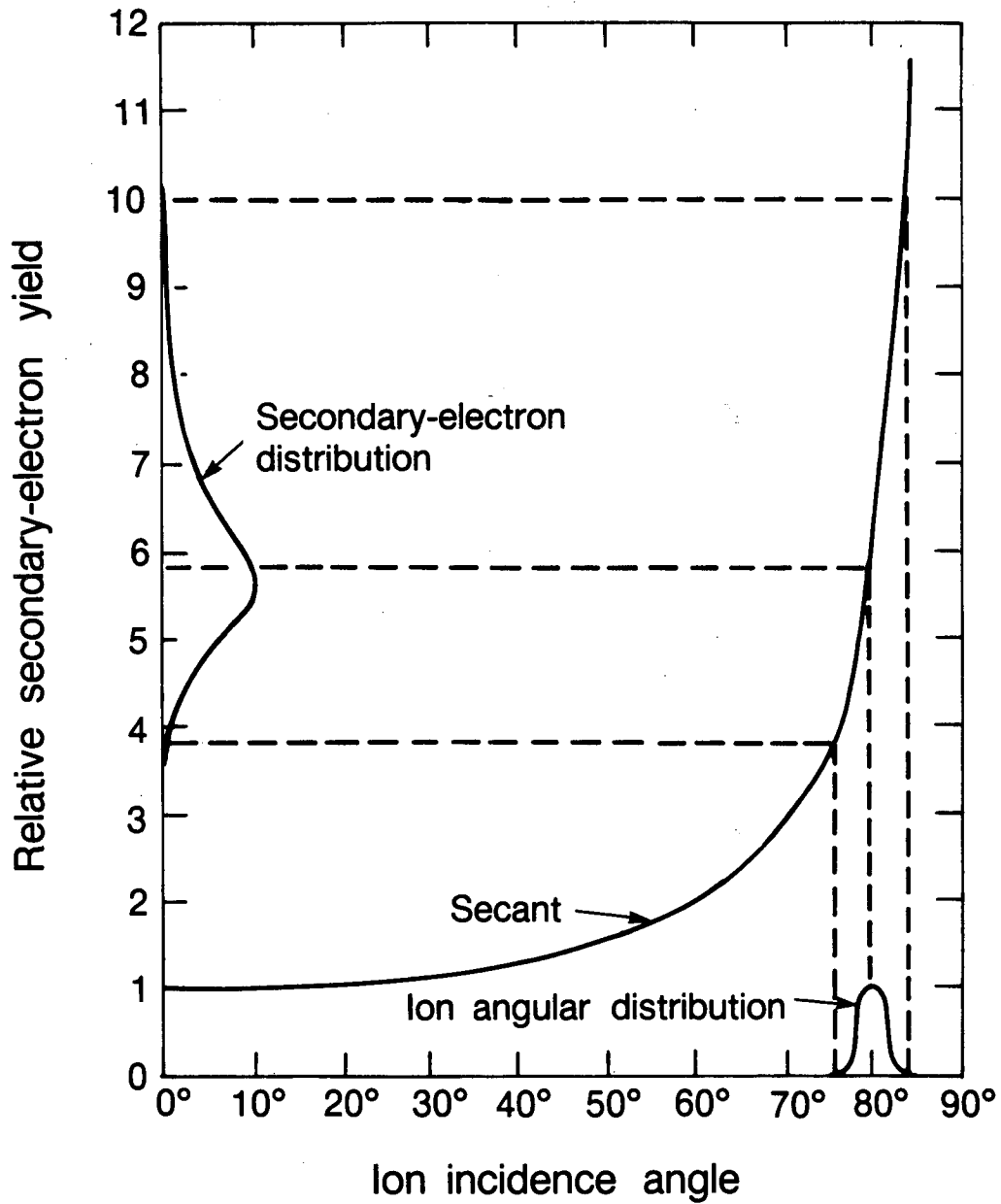
XBL 8610-11733

Figure 3.5   The secant dependence of the dynode yield on ion angle leads to skewed secondary-electron distributions. The effect is larger for lighter ions, which scatter more in the dynode. The distributions are not drawn to scale.

by the ion count rate and the electronic charge. In cases where we had no data on the output current, we measured the mean of the pulse-height distribution. We divided the mean by the previously calibrated number of pulse-height analyzer channels per secondary electron, to find the mean secondary-electron yield. Figure 3.6 compares these ion incidence-angle data to those of Dietz.[33] The agreement in secondary-electron yield at 80° is coincidental since the ion energy and species and the dynode surface preparation were different. However, the yield increase between 80.0° and 82.3° is consistent with the trend of Dietz' data up to 80.0°. We found no data in the literature for angles above 80°. Of the two other dynodes plotted in figure 3.6, our dynode surface is more similar in flatness and depth to the plasma-anodized surface. Figure 3.7 shows the secondary-electron yield dependence on ion species for this and previous data.[30,33,46] The results are qualitatively consistent after correcting for incidence angle. However, in spite of the fact that we took these data with higher ion energy and incidence angle, both of which should increase the secondary-electron yield, the yield is not much higher than Dietz's data at 80°. This indicates that further effort to optimize dynode preparation might increase the secondary-electron yield, allowing the use of a higher threshold to discriminate background.

Previous authors[30,47] have shown that for a given ion the secondary-electron yield is approximately proportional to ion velocity minus a threshold velocity of about 5×10^6 cm/sec. Figure 3.8 shows data for this detector before and after corrections to remove the effect of changes in actual incidence angle with ion velocity. The corrections are necessary because we did not adjust the orientation of the detector with respect to the beam to cancel the increased curvature of the lower-energy beam. We did adjust the slit position to center the beam on the dynode. We calculated the incidence angle for each velocity and made corrections to each data point for yield as a function of angle by interpolating the data, shown in figure 3.6, for this work and for Dietz's plasma-anodized
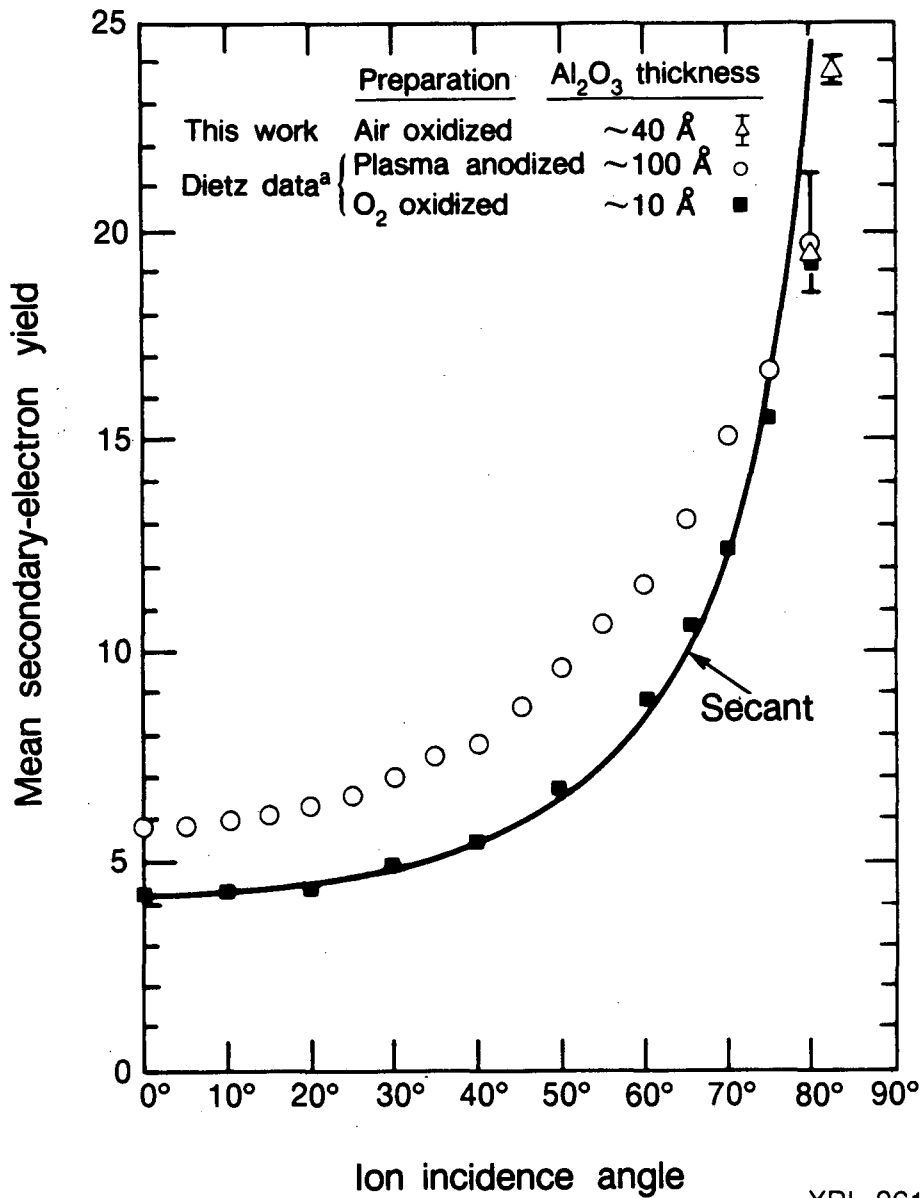
XBL 8610-11746

Figure 3.6   Data for mean secondary-electron yield as a function of ion incidence angle
are compared to the secant model discussed in section 3.3.1. The O_2 oxidized dynode
surface of Dietz [JJ6] is formed by depositing aluminum on a glass substrate. The flatness
and thinness of the resulting Al_2O_3 layer probably reduces the effective scatter of ion
angles with respect to the local normal to the surface and causes the yield to be close to the
secant dependence of the model. The agreement of the data from this detector for
41 keV [133]Cs^+ at 82.3°, with Dietz's data for 30 keV [85]Rb^+ at 80° is coincidental
(section 3.3.1).

	Ion energy	Incidence angle	Target	Reference
▼	41 keV	82.3°	Al_2O_3	This work
◉	30 keV	80°	BeO	Dietz[33]
○	30 keV	80°	Al_2O_3	Dietz[30]
■	40 keV	≈45°	Al	Daly[46]
▲	30 keV	0°	BeO	Dietz[33]
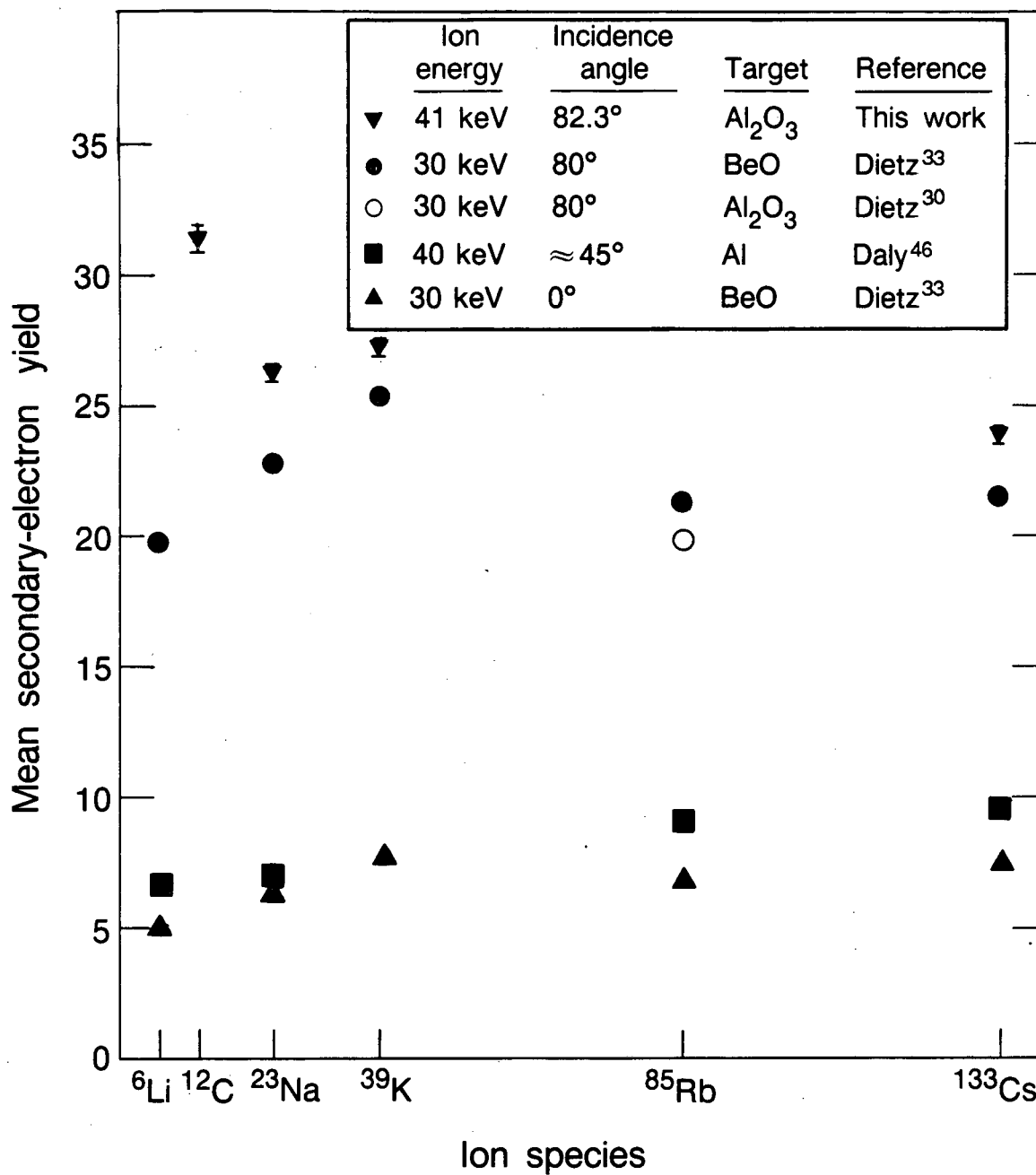
XBL 8610-11743

Figure 3.7   The mean secondary-electron yield is shown for positive alkali metal ions and $^{12}C^+$. For the data shown from this work, the ions approaching the detector had 40 keV but gained an additional 1 keV falling through the drift-gap field onto the dynode.

Ion energy (keV)
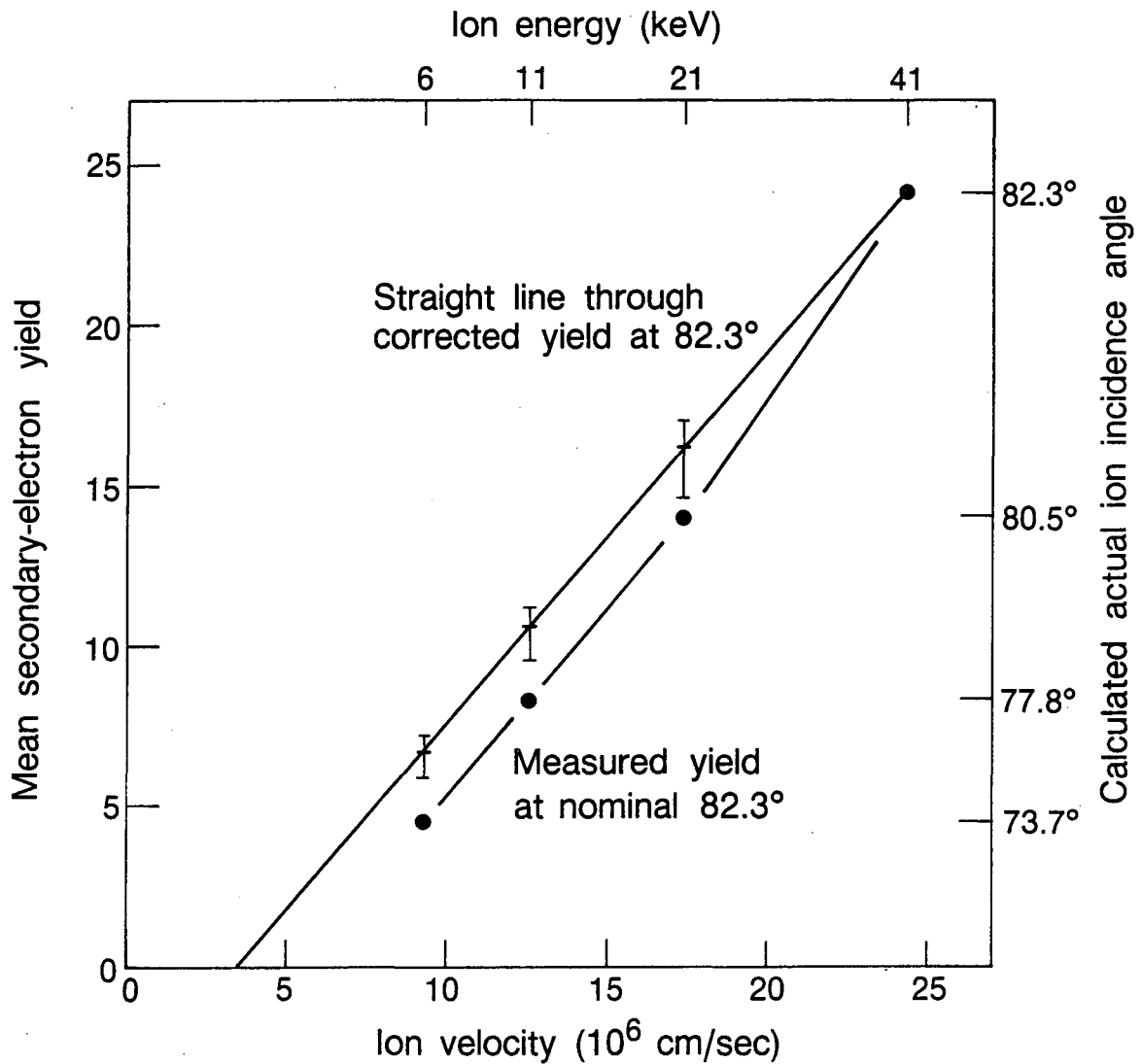
XBL 8610-11745

Figure 3.8   The mean secondary-electron yield as a function of ion velocity is shown for Cs$^+$ ions. The calculated actual incidence angle, shown on the right-hand axis, differed from the nominal angle of 82.3° as explained in section 3.3.1 of the text. Each data point (●) was corrected for the difference between the nominal and actual angle. The corrected yield (+) shows effect of velocity on yield at a fixed ion incidence angle of 82.3°. Given the large error bars, the fact that the corrected points fall on a straight line is coincidental. The actual energies and velocities at impact are shown. In all cases 1 keV of that energy was gained falling through the drift-gap field onto the dynode.

dynode. A straight-line fit to the corrected data in figure 3.8 gives a threshold velocity of $3.6 \times 10^6 \pm 0.7 \times 10^6$ cm/sec, slightly lower than the value quoted above.

In summary, the detector ion distribution appears to be proportional to the secondary-electron yield distribution as we expect. The detector response as a function of various ion parameters is consistent with other results in the literature.

3.4. Dark-noise and background pulse-height distributions and rates

Since background rejection is the critical criterion of detector performance, we must understand the detector's response to dark noise and background. We tested this response as follows. In order to measure the intrinsic noise of the detector, we eliminated as many noise sources as possible. The resulting output of the detector we call the dark noise, which is the lower limit of the background. In order study the detector's ability to reduce background rates by discrimination we introduced two sources of background, one at a time, into the mass spectrometer to simulate the background we might encounter in the cyclotrino. The sources we used were the UV lamp described in section 3.2, and ions (and perhaps some soft x rays) from an ion pump near the detector, which we turned on only for this purpose. We refer to these respectively as UV background and ion-pump background.

In this section we first present and discuss the dark-noise and background integral pulse-height distributions. These are plots of the number of counts per second above a given pulse height. Here we use the same pulse-height scale as described in previous sections for measurements after the second exposure to air. The vertical axis represents the dark-noise or background rate for a given discrimination threshold, that is, the integrated number of counts per second above that threshold in the respective pulse-height distribution (not shown). We show that there is an optimum value of V_m for achieving the

lowest dark-noise rates and that there is no advantage to using an additional, upper discrimination threshold. In section 3.4.1 we show the effect of discrimination on background rate. Finally we discuss the stability and sources of the dark noise in sections 3.4.2 and 3.4.3 respectively.

An ion pump near the mass-spectrometer ion source remained on during all measurements, including the dark-noise tests, except for measurements of the effect of the pump itself. To reach the detector, background from this pump had to travel about 5 m past two right angles, through the magnetic field in the 90° mass-spectrometer analyzer, and through the slit or around the mask 5 mm in front of the detector. When this pump was off, the pressure rose from the 10^{-9} Torr range by about two orders of magnitude during a 3×10^3 sec measurement. To be consistent, we kept the pump on during all measurements because we wished to avoid additional pressure rises during measurements of 10^4 to 10^5 sec. Two tests conducted before the first exposure to air with this pump off showed that there was more dark noise at small pulse heights but less dark noise at pulse heights larger than three or four secondary electrons. This increased the total dark-noise rate (of all pulses larger than about 0.3 secondary electrons) by 6%. However, it decreased the length of the tail of the integral pulse-height distribution by about 20%. Tests conducted after the second exposure to air show no such effect. We do not know the cause of this effect or its disappearance. If it were real, one might conjecture that with the pump on the better vacuum somehow reduced the total dark-noise rate but that a few ions from the pump reached the detector and made the larger pulses that extended the distribution's tail. However, since we saw it only in very early measurements and not in later tests, we are inclined to think that it was spurious or that we made a measurement error. If having the pump on during dark-noise tests does actually extend the distribution tail, then the true dark-noise level is below the values we measured.

Figure 3.9 compares the integral pulse-height distributions for dark noise at various V_m before the first exposure to air. Although the statistics are not conclusive, one can see that in general the dark-noise rate falls as V_m increases from 1.9 kV to 2.3 kV. It then rises again as V_m increases to 2.7 kV. Regardless of discrimination-threshold setting, $V_m = 2.3$ kV is optimal for the lowest dark noise. The reason that there is an optimum may be that at higher V_m there is more field emission but at lower V_m the single-electron distribution is less saturated, as the shape of the 1.9kV curve indicates. However, every microchannel-plate electron multiplier is different, and each would require individual optimization. In general, different V_m might be optimal at different discrimination thresholds. This is the case after the second exposure to air for the dark-noise measurements shown in figure 3.10. Here, $V_m = 2.3$ kV is still optimal for most discrimination thresholds. However, in a small region near one secondary electron, $V_m = 2.5$ kV gives slightly lower dark-noise rates. The small difference is statistically significant, although a systematic error in measuring the gain at each V_m might account for the difference by horizontally shifting the relative positions of the curves. Section 3.6 discusses the fact that the tail of the $V_m = 2.3$ kV dark-noise distribution is longer in figure 3.10, after the second exposure to air, than in figure 3.9.

For use in comparing background to signal, figure 3.10 includes the integral pulse-height distribution for 40 keV ^{133}Cs ions. Raising the discrimination threshold much above the point where the signal decreases relatively faster than the dark noise does not improve signal-to-noise. One can also see from figure 3.10 that there is no advantage to excluding counts above an upper discrimination threshold. Above any reasonable lower threshold the dark noise initially drops more steeply than the signal. The fraction of signal counts remaining above an upper threshold will always be larger than the fraction of dark-noise counts above that upper threshold. It would therefore be counterproductive to exclude counts above an upper discrimination threshold since this would cut out a larger

Error bars
2.3 kV Others
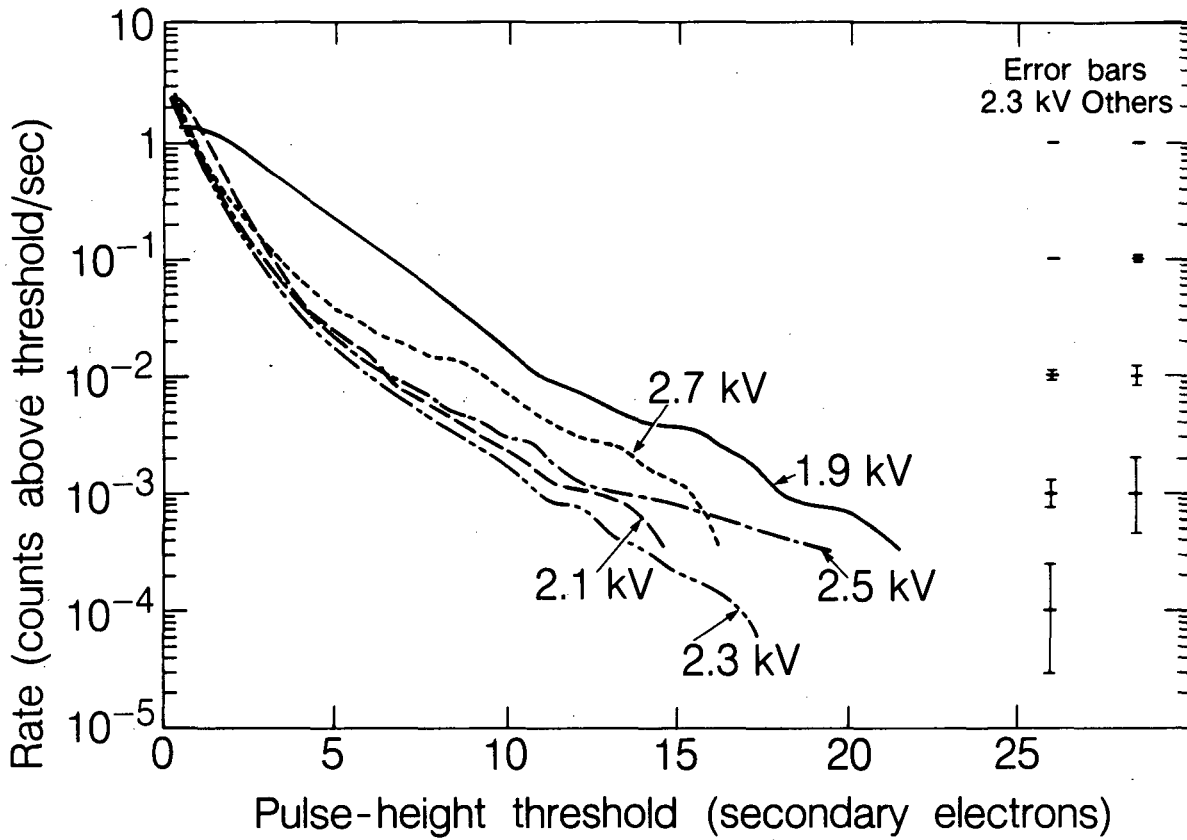
XBL 868-11657

Figure 3.9   The integral pulse-height distributions of dark noise are shown for various

values of V_m. The spline curves shown are fit through data points approximately one

secondary electron apart. Typical error bars are shown. The actual errors may be found

from the square root of the number of counts, which may be calculated from the rate on the

plot and the fact that the measurement times are 1.8×10^3 sec for the 2.3 kV data and

3.0×10^3 sec for the other data.
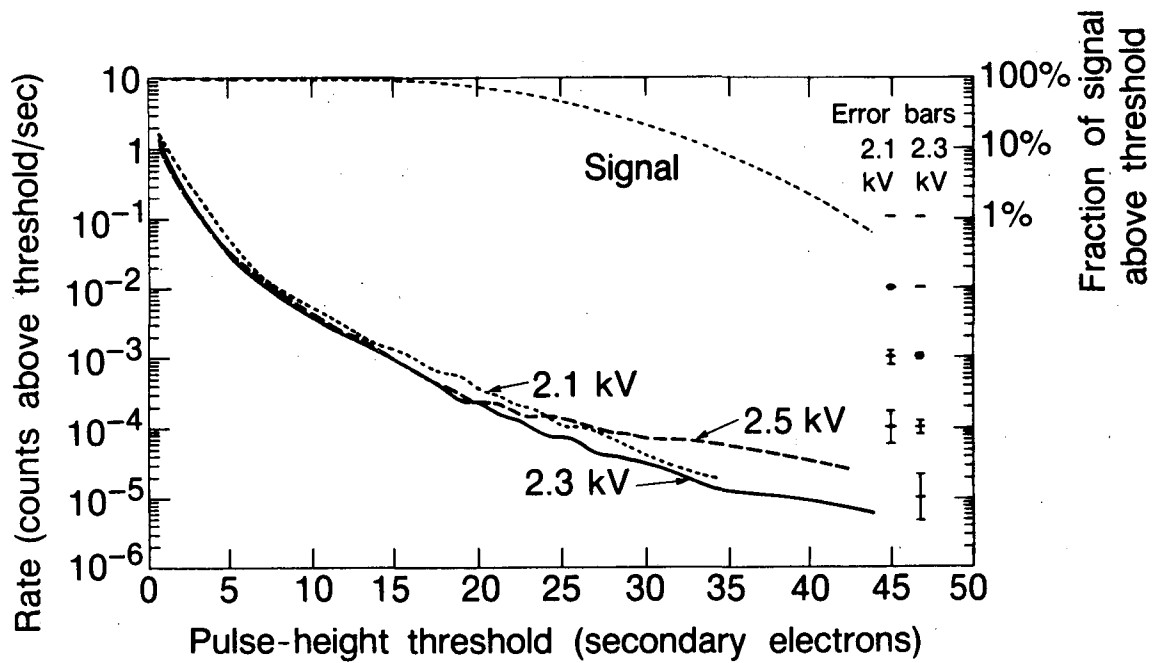
Figure 3.10   The integral pulse-height distributions, after the second exposure to air, are shown for the dark noise at various values of V_m and for the 40 keV ^{133}Cs$^+$ ion distribution at 2.3 kV. Typical error bars are shown. The spline curves shown are fit through data points approximately one secondary electron apart. The actual errors may be found as described in the caption for figure 3.9. The measurement times are 5.6×10^4, 2.8×10^5, and 7.7×10^4 sec, for the 2.1, 2.3, and 2.5 kV data respectively.

fraction of the signal than of the background.

3.4.1. Reduction of background by discrimination

Figure 3.11 shows integral pulse-height distributions for UV and ion-pump background tests, compared to the dark-noise distribution. Each background distribution includes detector dark noise. Above 9 secondary electrons for the UV background, and 15 secondary electrons for the ion-pump background, each background is within statistical uncertainty of dark noise alone. The three distributions were measured after the second exposure to air. The UV photons are from the 2537 Å mercury line (5e V). The ion-pump background has a maximum energy of 5 keV. We define the total background rate as the rate of pulses larger than 0.5 secondary electrons, the lowest discrimination threshold plotted. The fact that the total rate is higher for the UV background is due merely to the relative amounts of flux of the two backgrounds. The longer tail of the ion-pump background distribution is significant. We believe the reason for its length is that some of the background ions emit more than one secondary electron at the dynode. In order to find the fraction of background pulses that remain above a given discrimination threshold, we subtract the dark-noise distribution from each of the two background distributions, and normalize each total background rate to unity. The fractional reduction of background as a function of discrimination threshold is plotted in figure 3.12. The results are impressive. Discrimination reduces UV and low-energy ion backgrounds by five orders of magnitude at thresholds of 9 and 15 secondary electrons, respectively. The exponential decrease of each background is nearly constant. This indicates that their steep slopes may continue beyond the pulse height where our data lose statistical significance.

We took the data in figure 3.12 at $V_m = 2.3$ kV. One could repeat this test at other V_m to optimize the background reduction as described above for dark noise alone. We expect that $V_m = 2.3$ kV would be optimal in this case also, especially at higher
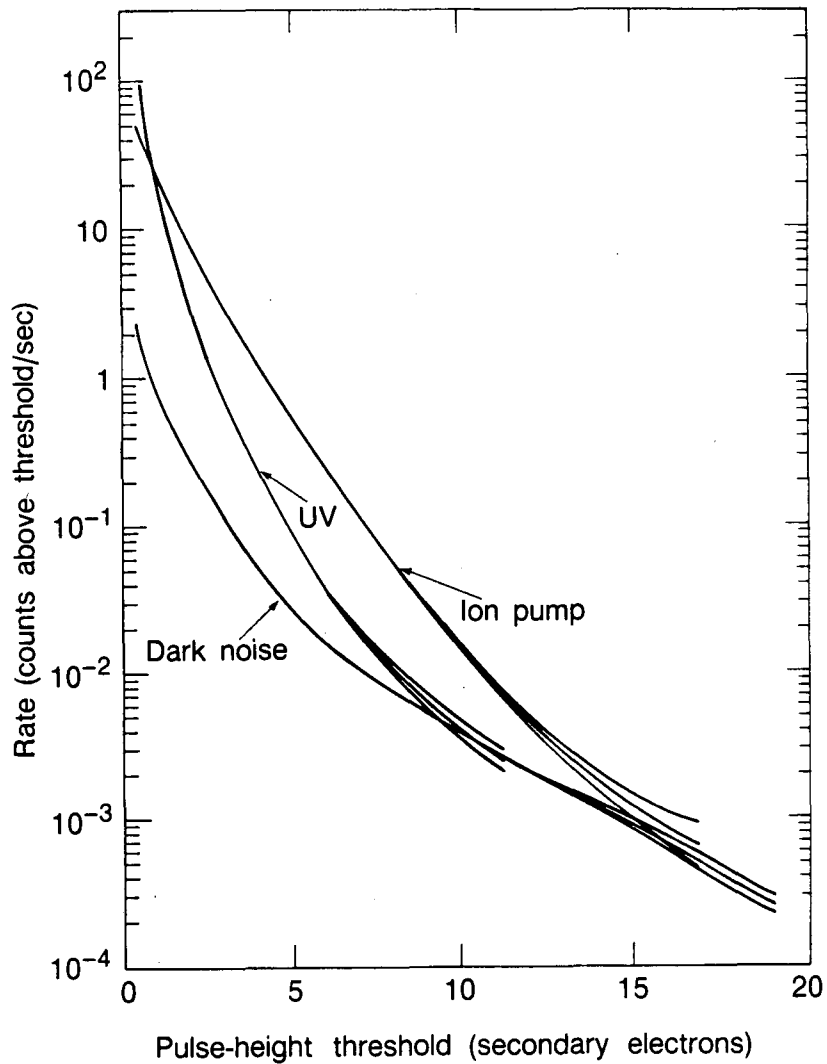
Figure 3.11   The integral pulse-height distributions are shown for the two simulated

backgrounds and the dark noise.   The spline curves shown are fit through data points

approximately one secondary electron apart.   For each curve the mean value and ± 1 σ are

shown.

XBL 8610-11750

Figure 3.12   Background reduction is shown as a function of pulse-height threshold. The curves shown are the integral pulse-height distributions for each of the backgrounds in figure 3.11 after subtracting the dark noise and normalizing to unity at 0.5 secondary electrons. The mean value and $\pm 1 \sigma$ are shown.

discrimination thresholds where the distribution of the background plus the dark noise approaches the distribution of the dark noise alone.

3.4.2. Dark-noise stability

The dark noise remained stable during tests in the mass spectrometer with three apparently unrelated exceptions. First, occasionally after an increase in V_m, the electron multiplier generated small, spontaneous pulses with a distribution that peaked at 0.25 secondary electrons, at rates up to 130 counts/sec. Second, in some measurements the dark-noise rate doubled at pulse heights above 14 secondary electrons, while remaining unchanged below that threshold. And, third, the gain and dark-noise distribution changed slightly as a result of exposure to air. We discuss this third exception in section 3.6. We saw no change in dark noise after operating the electron multiplier at output currents up to the nominal limit of 10% of the strip current, the quiescent current through the microchannel-plate stack (section 4.1).

We believe the spontaneous pulses result from microchannel-plate damage due to high-voltage discharge (section 3.7). We waited for the spontaneous pulses to subside (a few minutes to a few hours) before taking dark-noise data, so we do not know if their presence increased the dark-noise rate at pulse heights above a few secondary electrons. However, we believe that in one of the dark-noise measurements these pulses were present and increased the total dark-noise rate by 50%. Yet for pulse heights above one secondary electron the measured distribution was the same as other dark-noise distributions.

The dark-noise rate doubling above 14 secondary electrons occurred 3 times out of the 11 runs that were long enough to see the effect above statistical fluctuations. These were twice during dark-noise measurements, once each at $V_m = 2.3$ kV and $V_m = 2.5$ kV, and once during a UV background measurement at $V_m = 2.3$ kV. All are

shown in figure 3.13. For baseline comparisons, we plot as solid curves the sum of other dark-noise measurements at $V_m = 2.3\,\mathrm{kV}$ and the one dark-noise measurement at $V_m = 2.5\,\mathrm{kV}$. At the pulse height of 25 secondary electrons the rate doubling of the 2.5 kV dark-noise distribution disappears. This is significant at the 2σ level. The similar decline of the 2.3 kV dark-noise distribution at 28 secondary electrons is statistically insignificant. We believe the rate doubling is real because it is so similar in all three instances. We do not know the cause of the effect. It may result from intermittent electronics noise from elsewhere at the lab.

3.4.3. Sources of dark noise

The total dark-noise rate for pulses larger than 0.5 secondary electrons ranges from one to three hertz as V_m ranges from 1.9 to 2.7 kV, both before and after exposures to air. Electronics noise from sources such as the amplifier do not contribute because, unlike other dark noise, it is not multiplied by the high-gain electron multiplier and therefore its pulse height remains smaller than 0.5 secondary electrons. In pulse-counting mode, the gain was always high enough that electronics noise did not appear above the lowest pulse-height analyzer channel when the analyzer and the amplifier were set so the 40 keV ion distribution peaked around channel 100 (≈ 25 secondary electrons). For the F4129 phototube Lo and Leskovar[27] tested, the dark noise from the stack, with the photocathode backbiased, was 5 counts/sec with $V_m = 2.4\,\mathrm{kV}$, and a threshold of 0.13 secondary electrons. We believe the cause of dark noise at small pulse heights is thermal and field emission of electrons. One expects the mean height of such pulses to be one secondary electron or less depending on whether the electrons are emitted at the dynode or in a microchannel-plate pore. Figures 3.9 and 3.10 show that most dark noise is indeed near or below the pulse height of one secondary electron.

Although most dark-noise pulses are small, figure 3.10 shows that the dark-noise
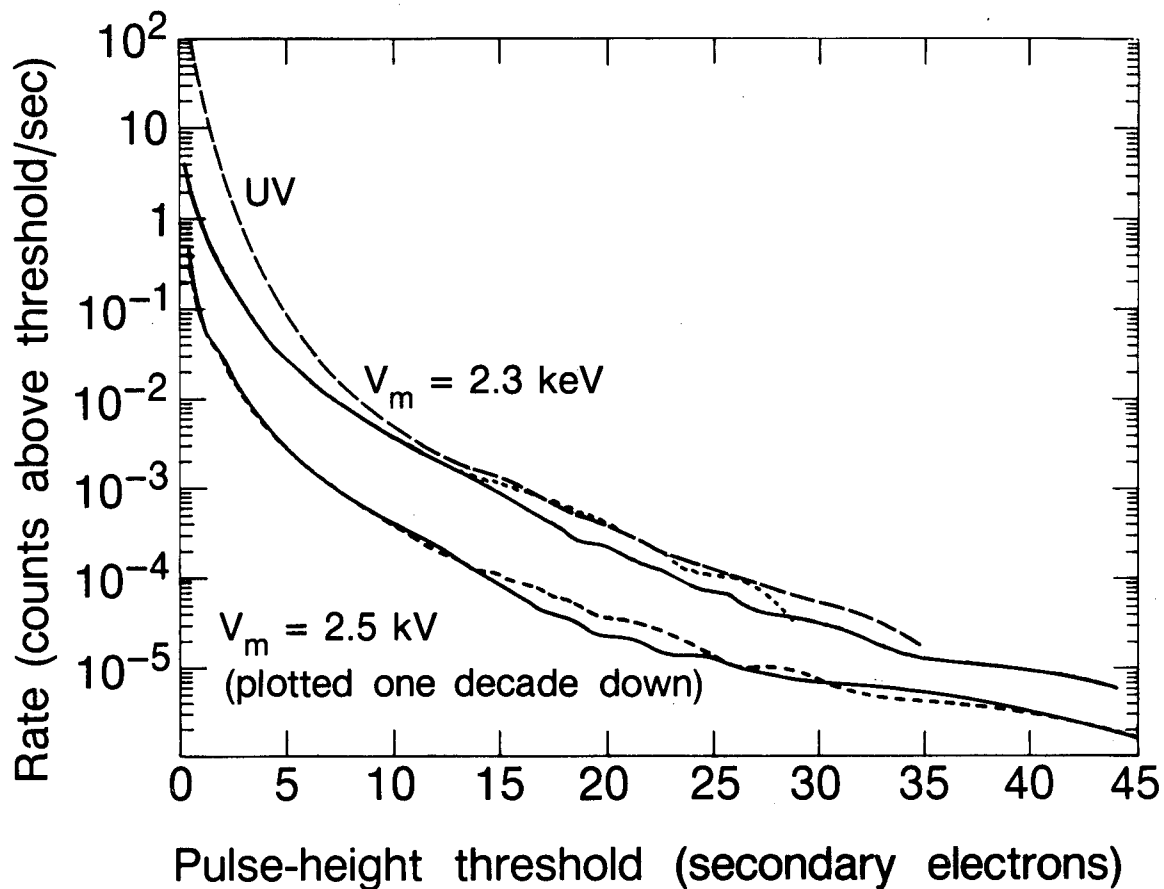
XBL 8610-11742

Figure 3.13   These integral pulse-height distributions of dark noise and UV background

show a twofold increase in background rate at pulse heights above 14 secondary electrons.

The solid curves are typical dark-noise distributions shown for comparison as baselines.

The 2.5 kV data is plotted one decade down for visual clarity.   The statistical significance

of the background-rate increase is discussed in section 3.4.2.

distribution has a tail which extends beyond 40 secondary electrons at $< 10^{-5}$ counts/sec. We believe the causes of these infrequent, large dark-noise pulses in this detector are similar to the causes of such pulses in standard photomultiplier tubes.[48,49] The large pulses are of two types: those that are intrinsically large and those that are due to fluctuations in multiplier gain which cause a field emission event to be amplified by the multiplier to an unusually large size. Possible sources of intrinsically large pulses, which fire many pores, include cosmic rays, intrinsic radioactivity (^{40}K in glass), high-voltage discharge, ion or photon feedback,[50] and bursts of molecular ions and photons from ion pumps that arrive at the detector within the time constant of the discrimination electronics.

In general, statistical fluctuations in electron-multiplier gain are due to random microscopic multiplication processes. The distribution of fluctuations is broadened by nonuniformity of multiplication surfaces and, in the case of microchannel plates, differences in the number of pores fired and differences in effective number of dynodes from pore to pore. The distribution is also affected by the extent to which the electron-multiplier gain is saturated and by the number of broken or malformed pores and the details of the random stacking of the three microchannel plates. Geometrically, on the basis of random stacking, no more than thirteen pores can be fired in the output plate for a single pore fired in the input plate,[26] but if the plates were warped or damaged, this number might be larger.

Dietz has written extensively on the application of Polya statistics to ion detectors.[17,30,31,51,52,53,54,] According to Dietz, the Poisson distributions for the probable gain at each point on a multiplication surface combine into a Polya distribution for the overall gain. The Polya distribution is broader than the Poisson distribution, so on a statistical basis alone one expects the dark-noise distribution to drop off less quickly than the tail of a Poisson distribution.

3.5. Ion-counting efficiency versus dark-noise and background rates

In sections 3.3 and 3.4 we discussed the pulse-height distributions of the ion signals, and of the dark-noise and background rates as functions of discrimination threshold. In this section we first discuss ion-counting efficiency as a function of discrimination threshold. Then we compare ion distributions to dark-noise and background distributions to find dark-noise and background rates, as direct functions of ion-counting efficiency, by eliminating discrimination threshold as the independent variable. In making this comparison we assume that dark-noise and background distributions are unaffected by detection of signal ions. We believe this is true at least up to ion count rates of between 10^2 to 10^3 ions/sec (depending on electron-multiplier gain) at which we took the ion data discussed in this section. The quantitative similarity of the background to the left of the valley in ion distributions, to the dark-noise distribution, is consistent with this hypothesis.

In this section we analyze data taken at $V_m = 2.3$ kV, which was found in section 3.4 to be optimal for low dark-noise rates at thresholds above one secondary electron. In theory, differences in ion-counting efficiency versus threshold for particular ions could cause other V_m to have a lower dark-noise rate as a function of counting efficiency at particular values of counting efficiency. The data show that $V_m = 2.3$ kV remains optimal in general. Section 3.5.1 discusses the exceptions.

We define the counting efficiency as the ratio of the ions that make pulses larger than a given discrimination threshold, to the total number of ions hitting the dynode that make a non-zero pulse-height signal. This neglects the few ions for which no secondary electrons are collected. The fact that background-subtracted ion distributions (not shown in a figure) have low amplitudes at pulse heights near zero indicates that there is not a second

population of ion pulses at very low pulse heights. If the beam extended beyond the edge of the dynode, some of the secondary electrons that were emitted by ions hitting near the edge would be lost. This would broaden the ion distribution toward lower pulse heights, reduce the peak-to-valley ratio, and increase the amplitude of the background-subtracted ion distributions near zero pulse height. There is no indication that the beam extended beyond the dynode during tests in the mass spectrometer. However, an increase in ions hitting near the edge of the dynode may have caused a reduction of the peak-to-valley ratio observed in the cyclotrino.

In order to be sure that our counting efficiency measurements are valid we must scrutinize the validity of our assumption that essentially all ions make signals with pulse heights greater than zero. The following shows that a negligible portion of beam ions with 5 keV or more energy emit no secondary electrons. That is, the ion-counting efficiency is nearly 100% at a discrimination threshold near zero. Thus the ion pulse-height distributions in figure 3.4 represent essentially all the ions, as well as the background. The 5 keV ions, the lowest energy tested, are most likely to emit zero secondary electrons. An average of 4.3 secondary electrons are collected from a 5 keV Cs ion, in a distribution which we expect to be no narrower than a Poisson distribution. Therefore the probability of collecting zero secondary electrons must be at least as large as the 1.4% probability of measuring zero given a Poisson distribution with a mean of 4.3. For 10 keV Cs ions the average number of secondary electrons collected is 8.1, so the Poisson lower limit on the fraction of ions for which zero secondary electrons are collected is 3×10^{-4}. After subtracting background, the data in figure 3.4(c) is consistent with values near these lower limits.

Figure 3.14 graphs dark-noise rate (plotted on a log scale) against ion-counting efficiency (plotted on a log-log scale) for various ions at 82.3° incidence angle. We took
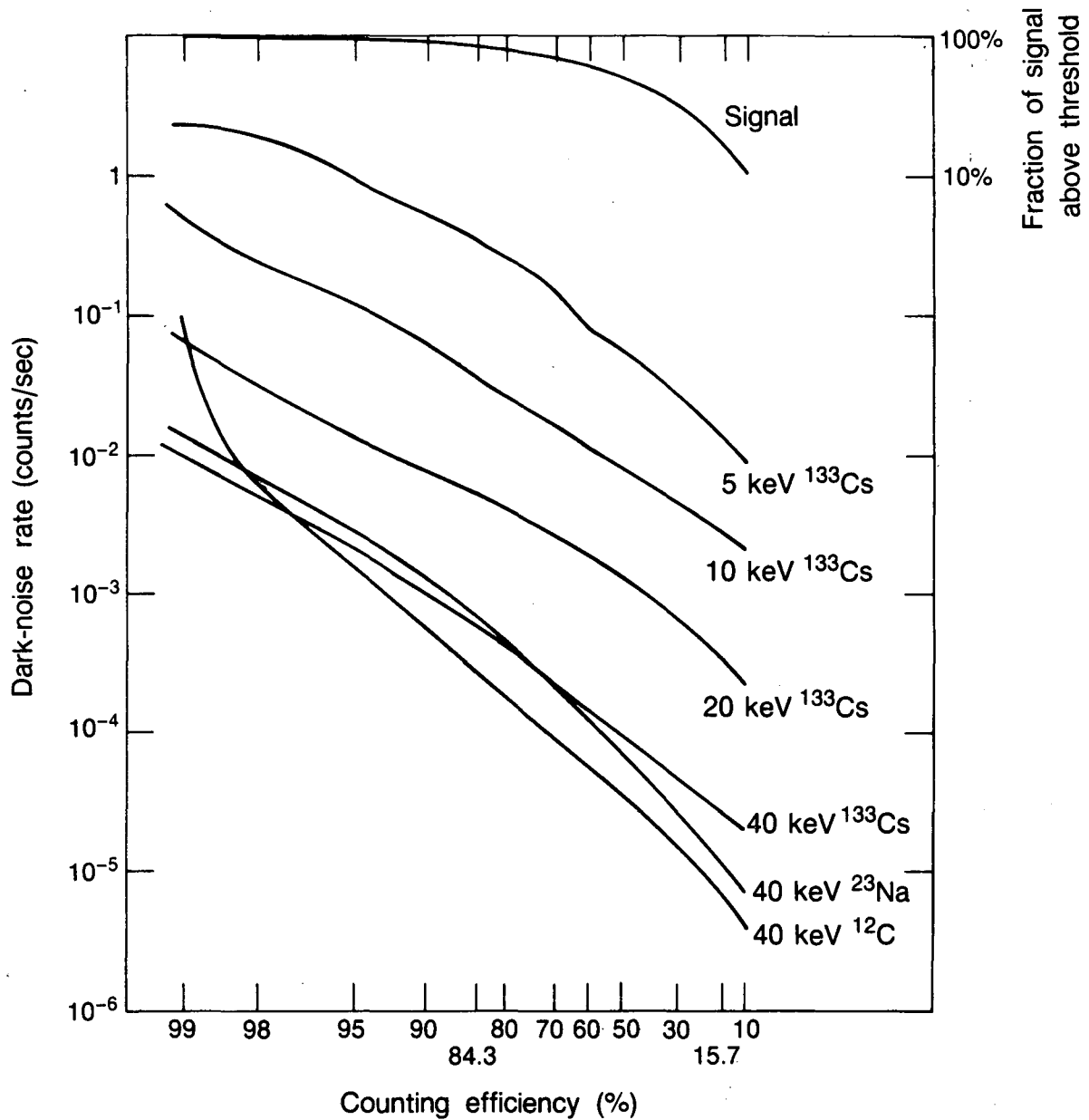
Figure 3.14   This plot indicates the overall performance of the detector with respect to dark noise versus counting efficiency. All data shown is for ions at 82.3° nominal incidence angle but for the 5, 10, and 20 keV data the actual incidence angles are lower as explained in section 3.3.1. Thus the increase in the dark-noise rate for lower energies is due in part to the smaller angles. The curve labeled "signal" is the counting efficiency for 40 keV ^{133}Cs$^+$ plotted against itself, for comparison to the dark noise.

these data after the second exposure to air, with $V_m = 2.3 \, \text{kV}$. Figure 3.14 is derived from the ion and dark-noise data shown in figures 3.4(b), 3.4(c), and 3.10. A curve showing the fraction of signal pulses above the threshold is also plotted on figure 3.14 for use in comparing the signal to noise for different choices of counting efficiency. This is equivalent to plotting the counting efficiency against itself.

Figure 3.14 clearly demonstrates the tradeoff between dark-noise and counting efficiency. By sacrificing some counting efficiency the detector can achieve very low dark-noise rates. The figure also shows the improvement of both dark-noise and counting efficiency with increased ion energy. The dark-noise rate decreases by a factor of eight or nine at the same counting efficiency with each doubling of energy. The discrimination threshold required for counting efficiencies above 97% is lower for carbon than for cesium at the same 40 keV energy. This is because the ion distribution for carbon is wider than that for cesium (figure 3.4(b)), so a larger fraction of it is at low pulse height. Thus for any given counting efficiency in the range above 97% the dark-noise rate is higher for carbon than for cesium, as figure 3.14 shows. Conversely, the dark-noise rate is lower for carbon at counting efficiencies below 97% because the mean pulse height of the ion distribution for carbon is higher than for cesium.

The data in figure 3.14 show that in the mass spectrometer we were able to detect 36 keV carbon ions at 50% efficiency with a dark-noise rate of 5×10^{-5} counts/sec. The best we could hope to do in the cyclotrino would be to suppress the background to the level of dark noise alone. In fact, to increase the effective dynode area in the cyclotrino, we chose to use a less-grazing ion-incidence angle, about 75°, compared to 82.3° for this data. This is less advantageous insofar as the median pulse height of the carbon ion distribution should be about 40% lower, or about 18 secondary electrons. The correction for detecting $^{14}C^-$ instead of $^{12}C^+$ is small by comparison. In the cyclotrino we operate at

$V_m \approx 2.0\,\text{kV}$. Thus the dark-noise rate should be a little above 7×10^{-4} counts/sec $\pm 16\%$, which is the value for $V_m = 2.1\,\text{kV}$ in figure 3.10. If the background in the cyclotrino is similar to the ion-pump background, figure 3.12 indicates that a discrimination threshold of 18 secondary electrons should reduce its unknown rate by $\sim 10^6$. In fact we obtained a background rate in the cyclotrino, at 50% counting efficiency, of 6×10^{-4} counts/sec $\pm 10\%$, which is in agreement with the expected dark-noise rate to within the errors. This indicates that the detector is successful at reducing the cyclotrino background rate to nearly the rate of the dark-noise alone.

Figure 3.15 plots background reduction data (from figure 3.12) against counting efficiency, for $40\,\text{keV}\ ^{12}\text{C}^+$ and $^{133}\text{Cs}^+$, at 82.3° ion incidence angle, with $V_m = 2.3\,\text{kV}$. The detector can provide large reductions of background even at 99% counting efficiency.

3.5.1. Other criteria for choosing microchannel-plate voltage

There are three cases when one might prefer a different V_m to that found to be optimal for reducing the dark-noise rate (2.3 kV for this particular electron multiplier, section 3.4). First, if one wishes to count ions at a rate exceeding that allowed by the maximum anode current at $V_m = 2.3\,\text{kV}$ (section 4.1), one must reduce V_m in order to decrease the electron-multiplier gain. Second, it is possible that if the electron multiplier were operated for additional time at $V_m > 2.3\,\text{kV}$, the dark-noise rate might decrease at those V_m. As V_m is increased to a higher value for the first time, the dark-noise rate distribution increases initially, then decreases asymptotically to an apparently stationary distribution. We did not study the time dependence of this decrease. We have operated the electron multiplier a total of about 500 hours, mostly at $V_m = 2.3\,\text{kV}$. For less than one tenth of this time was $V_m > 2.3\,\text{kV}$.
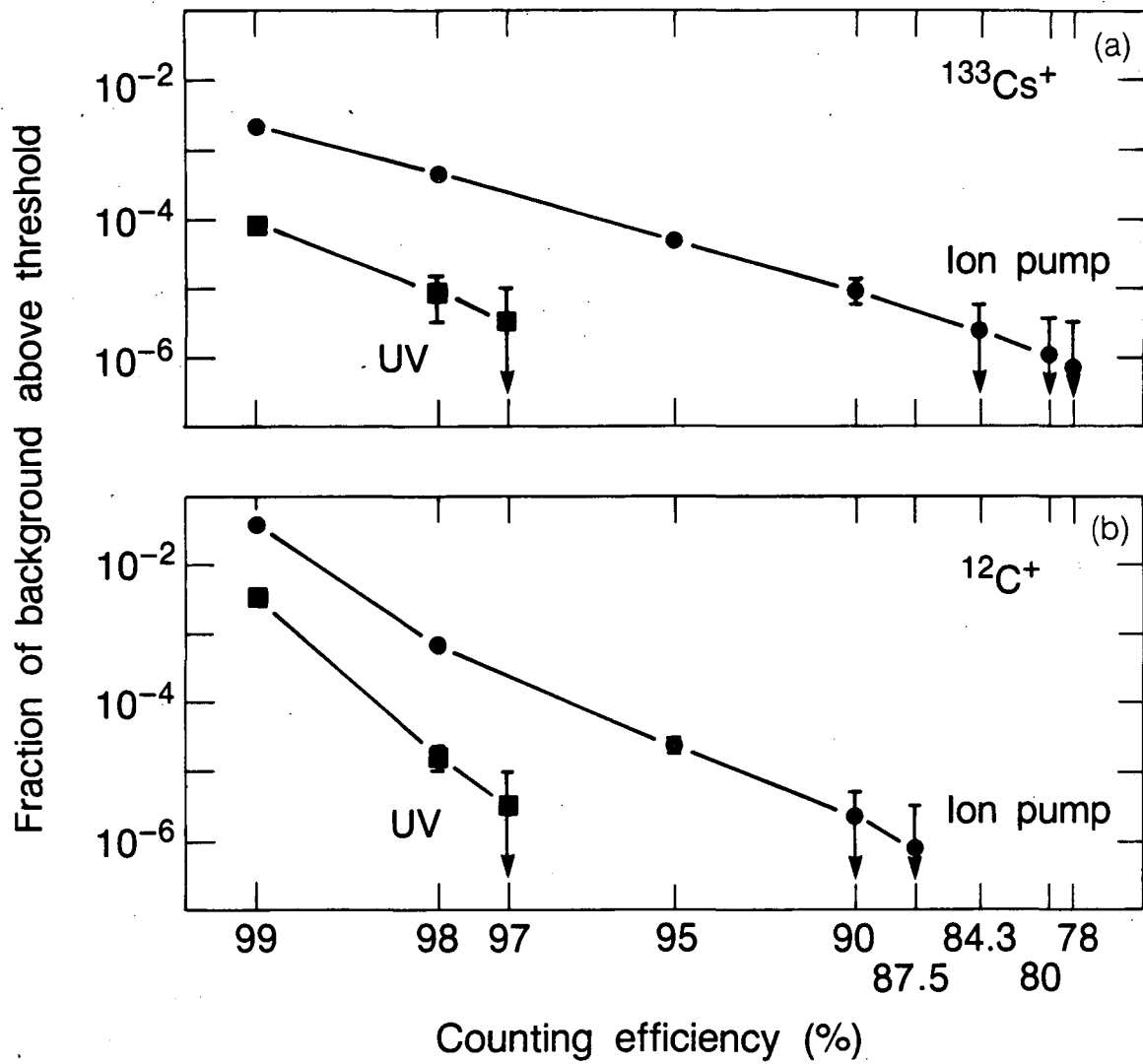
Figure 3.15 The fractional reduction of background is plotted against counting efficiency for $40\,\text{keV}$ $^{133}\text{Cs}^+$ (a) and $40\,\text{keV}$ $^{12}\text{C}^+$ (b), both at $82.3°$. The detector exhibits excellent background discrimination.

Third, although the dark rate distribution is slightly higher for $V_m > 2.3$ kV, the ion distribution is slightly narrower because the greater microchannel-plate saturation at higher V_m narrows the single-electron distribution. For counting efficiencies greater than about 50%, this raises the discrimination threshold, in units of secondary electrons, required to achieve a given counting efficiency. This is shown schematically in figure 3.16. Thus, for a given counting efficiency (though not for the same discrimination threshold), the dark-noise rate can be lower for $V_m > 2.3$ kV. This effect is more pronounced at higher counting efficiencies. In these data the most extreme example is for counting 40 keV Cs with 99% efficiency. In this case, the discrimination threshold with $V_m = 2.3$ kV is 7.2 ± 0.2 secondary electrons, while the threshold with $V_m = 2.7$ kV is 9.1 ± 0.2 secondary electrons. Although we did not measure the dark rate with $V_m = 2.7$ kV after the second exposure to air, measurements at 2.3 and 2.5 kV indicate that the increase in discrimination threshold at 2.7 kV could decrease the dark rate at 99% efficiency by a factor of two for this example.

3.6. Stability of gain, signal, and background, after exposure to high currents or air

When a known gain change occurs in an electron multiplier used in an ion detector, it is typically not a problem. As long as the background distribution does not change relative to the signal distribution, this merely requires a recalibration of the appropriate discrimination thresholds. The distributions should remain essentially unchanged in units of secondary-electrons. In contrast, it is important that the dynode secondary-electron yield not decrease. If this occurs, or if something else reduces the pulse height of the signal relative to the background, the background rate would increase at a given counting efficiency. This would be a change comparable to what figure 3.14 shows for decreased ion energy, which reduces the dynode secondary-electron yield but does not affect the dark noise.
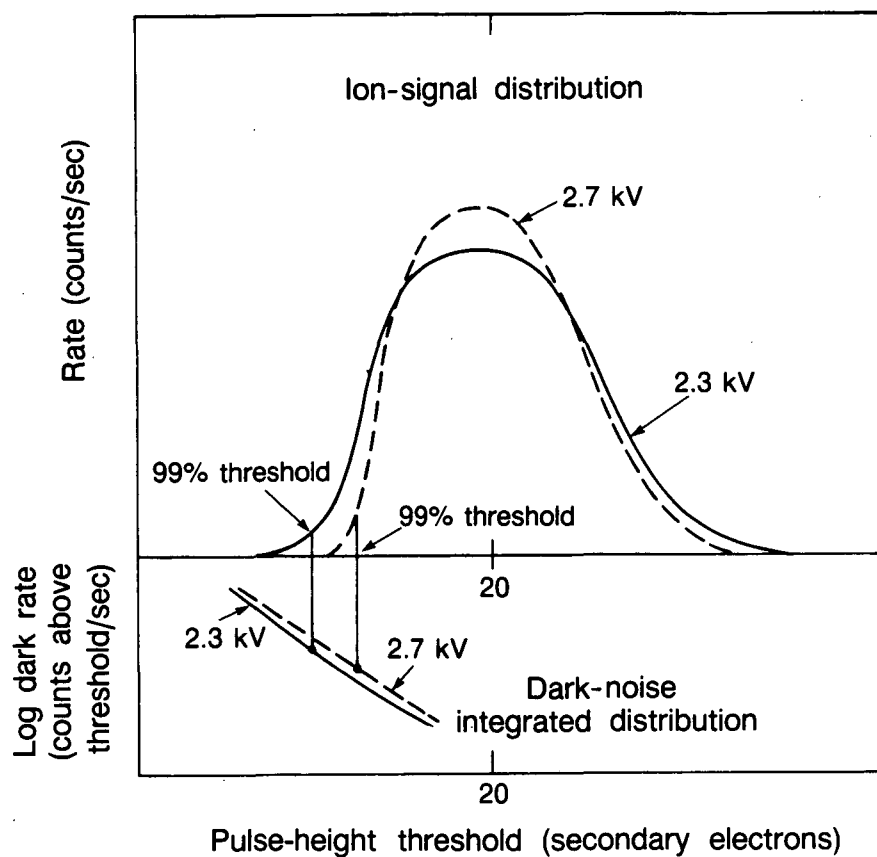
Figure 3.16   This drawing (not to scale) illustrates that a narrower ion-signal distribution can reduce the dark-noise rate at the discrimination threshold corresponding to a given counting efficiency, even when the narrower distribution is accompanied by a higher overall dark-noise or background distribution. Thus for counting efficiencies well above 50% it can be advantageous to use a higher choice of Vm. In this example the thresholds for 99% counting efficiency are shown.

During detector measurements we have seen decreases in electron-multiplier gain correlated with exposure to air or high ion-input and anode currents,[43] in addition to the 1% - 5% drift in the ion distribution mean, noted in section 3.3. In the mass spectrometer, immediately following the gain tests described in section 3.2.2, the signal pulse height decreased by 59%, but recovered to previous levels by the following day when we next tested it. During these tests ion rates reached above 10^{10} counts/sec, four or five orders of magnitude above any other tests in the mass spectrometer, and the anode current reached at least a factor of two above the nominal limit (section 4.1), perhaps much higher. In the cyclotrino the detector has been run at ion currents high enough to cause anode currents an order of magnitude or more above the nominal limit. Following high currents the gain takes a few minutes to several hours to rise to its previous level.

One of the reasons we chose a microchannel-plate electron multiplier for this detector was that we could expose it to air without its losing most of its gain and requiring reactivation of the multiplication surfaces. However, the microchannel-plate gain typically decreases over its lifetime.[39,43] A process similar to the electron scrubbing described in section 3.2.2 continues to decrease the secondary-electron yield of the pore surface as charge is extracted from the multiplier. In addition, when the gain is first turned up after each exposure to air, desorbed gas fires pores, scrubbing the microchannel plates a large amount at once. The manufacturer's entire electron scrub process decreases the gain several orders of magnitude at a given V_m, as one can see in figure 3.3. High gains can still be reached, with more complete saturation than before the scrub, by using higher V_m. However, one might prefer to use the same V_m if it were found to be optimum for the lowest dark-noise rate. Using a lower gain following an exposure to air should, in general, present no problem in this detector since the gain is so high in the unscrubbed electron multiplier to start with.

In the mass spectrometer the results of exposure to air were ambiguous due to disagreement between early UV measurements of the gain. After early tests, two exposures to air appear to have permanently reduced the gain of the detector by a total of $(21 \, {}^{+5}_{-10})\%$ as measured using the UV source. (No useful data exists from between the two exposures.) However, contrary to our expectations the absolute dark-noise distribution, in pulse height units of absolute charge, decreased by only $(2 \pm 2)\%$. Thus, in units of secondary electrons, the dark-noise distribution had a $(23 \, {}^{+7}_{-13})\%$ longer tail after the exposures to air. This increased the dark-noise rate at a fixed threshold, as one can see by comparing the $V_m = 2.3 \, \text{kV}$ curves in figures 3.9 and 3.10.

We do not understand why the pulse height of the dark noise did not decrease in proportion to the gain decrease. If the dark-noise increase is real it represents a decline in the performance of the detector that could prove to be a serious problem after repeated exposures to air. The apparent decline in detector performance in the mass spectrometer may be a spurious result, perhaps due to our inexperience with the equipment during early measurements. In any case, the results for dark-noise and background rates as a function of counting efficiency quoted in section 3.5 are based on data taken after the two exposures to air in the mass spectrometer. They are independent of any measurement errors before the exposures, and if the decline is real, they are post-decline results.

In the cyclotrino all efforts have so far been directed to making tail rejection measurements and little time has been spent measuring the detector's performance, so the following are impressions only. The detector has been exposed to air between 6 and 12 times since being installed in the cyclotrino. During this time the electron-multiplier gain, at $V_m = 2.0 \, \text{kV}$, decreased by a factor of about two. Over the same period, the peak-to-valley ratio for the pulse-height distribution for the sum of the signal and the background decreased from about 5 to about 1.3 during tests in the cyclotrino. This

indicates that again, contrary to our expectations, the pulse height of the background seems not to have decreased as much as that of the ion distribution. This required us to increase the discrimination threshold, resulting in lower ion-counting efficiency ($< 50\%$), in order to maintain a background rate of 6×10^{-4} counts/sec.

If this problem is the same ongoing problem we saw in the mass spectrometer, we must solve it in order to continue using the detector in the cyclotrino. It may also be hoped that the symptoms in the mass-spectrometer tests were spurious and that we can explain and easily fix the problem in the cyclotrino. One possible explanation is that something such as hydrocarbons from the internal ion source or pump oil contaminated the dynode surface and reduced the secondary-electron yield. The solution would then be merely to change the dynode. The external ion source should provide a cleaner vacuum.

A second explanation depends on the fact that in the cyclotrino we found electronics noise to be a major source of background, unlike in the mass spectrometer where electronics noise was negligible. This is due both to the presence of radio-frequency high-voltage and to the use of a lower V_m setting, which reduces the electron-multiplier gain by a factor of at least six from the final mass-spectrometer value. It is possible that as the gain continues to fall with repeated exposures to air, the pulse heights of the background and the ion distributions decrease proportionally, as expected, except for the electronics noise, which is constant in pulse-height units of absolute charge. The solution is to shield the detector from the noise or to increase the gain by operating at a higher V_m. The reason for operating at a lower V_m is to allow ion-counting rates up to several thousand ions/sec. We could operate at higher V_m to obtain low background rates when we count ions at low rates, and raise V_m whenever we need to count at ions at higher rates, when higher background rates are acceptable. This approach should continue to work as the electron multiplier ages. The only way to find out is to try it. We could also obtain an

electron multiplier with a higher strip current, which would permit a higher anode current limit for a given V_m (section 4.1). A last resort would be to operate above the limit and calibrate the gain as a function of ion current, taking hysteresis into account. We would prefer to avoid this last, inelegant solution. We need to study further the effects of exposure to air on background rate and counting efficiency, after turning on the cyclotrino in its new external source configuration (section 1.1.1).

3.6.1. Experience and suggestions about exposure to air

The following is a history of our experience with the results of exposure to air. The manufacturer delivered the electron multiplier in the vacuum vessel shown in figure 1.2. We opened the vacuum vessel and attached the electron multiplier to the rest of the detector under flowing dry nitrogen. We transferred the detector, using a plastic bag filled with dry nitrogen, into the mass spectrometer's vacuum with the detector's sliding door shut and little exposure of the microchannel plate to air. We pumped the detector down for several days before turning up V_m over a period of weeks to a maximum of 2.7 kV.

After operating the detector over a period of a few months we took it out into air for 18 minutes, then returned it to vacuum. After pumping down for 23 hours, we gradually increased V_m over 6 hours with no apparent ill effects, except a possible reduction in gain, but we took no useful data before the next exposure to air. Three days later we took the detector out of vacuum for 10 minutes and adjusted its orientation for a new ion incidence angle before returning it to vacuum. We pumped down for 18 hours before turning up V_m. After 2.5 hours at $V_m = 1.9$ kV and 4.75 hours at 2.1 kV the detector produced small, spontaneous pulses. We believe that these pulses are unrelated to the exposure to air but were brought on by turning up V_m and are a result of the damage described in section 3.7.

The detector can be pumped down and V_m turned up to operating level more quickly than described above. In the cyclotrino we introduce one atmosphere of dry nitrogen into the vacuum vessel before opening it to air. We are not sure to what extent this is beneficial but it may reduce the amount of water adsorbed on the microchannel-plate pore walls. After closing the vacuum vessel we pumped the detector down for about 5 hours before immediately turning the voltage up to 2.0 kV. An even shorter pumping time may be possible. The pumping time required probably depends on the amount of water adsorbed. The pores in the middle microchannel plate are the part of the detector that takes the longest to pump out. The Al_2O_3 dynode should not be affected by air (section 2.6).

We suggest three possible methods to avoid gain reduction after exposure to air. First, pump down longer before turning up the voltage. Second, remove the detector into a dry nitrogen atmosphere, instead of into air. Third, bake the electron multiplier to desorb water and gas before V_m is turned up. This might be done by installing a resistive heater around the body of the electron multiplier or directly to the metal post that supports the anode. During processing the manufacturer bakes the plates at 300 to 350°C, so baking to desorb gas at 200°C, sufficient to desorb most water and other gas, should not cause any problems. Malina and Coburn[43] have tested the second and third methods with varied results. Another possibility is to use an electron multiplier with microchannel plates that have been electron scrubbed by the manufacturer. This reduces and stabilizes the gain and makes it uniform over the active area. The effects of further scrubbing should be much smaller.[43]

3.7. Damage to electron multiplier from high-voltage discharge

During early tests in the mass spectrometer, a sudden current load caused the high-voltage supplies to both ends of the microchannel-plate to trip off as we tried to increase the voltage V_d between the dynode and the microchannel face from 2 kV to 3 kV.

We believe that a piece of dust, found later on the dynode, caused a high-voltage discharge between the dynode and the microchannel face that tripped the supplies. After this discharge, spontaneous pulses appeared in the dark-noise pulse-height distribution with a peak at about 0.25 secondary electrons. Initially the rate of these pulses was 300 counts/sec but by the next day it had fallen to about 10 counts/sec. After that the pulses stopped but reappeared occasionally at rates between 10 and 130 counts/sec for the duration of a few minutes to a few hours. They reappeared 20 to 30 times over a five-month period of almost daily use. The spontaneous pulses are probably caused by field emission. Other investigators refer to similar pulses as hot spots.[43,55] In one instance spontaneous pulses appeared at about 2×10^3 counts/sec in a distribution that decreased approximately linearly from 200 counts/sec in the lowest channel to near zero at about 0.2 secondary electrons. However, these may have been unrelated electronics noise.

We believe that the spontaneous pulses come from local damage in the microchannel plates caused when high current density melted or cracked part of the glass during the initial discharge that tripped the supplies. The evidence for this is that the pulses usually appear only after we increase the microchannel-plate voltage V_m, which should not cause field emission from dust on the dynode. The damage occurred before the first exposure to air and before we made measurements for any of the results we present in this work.

The high-voltage discharge hit the first plate, but one would expect the output plate to bear the damage because the current is multiplied by the first and second plates. The fact that the pulse height of the spontaneous pulses is about 0.25 secondary electrons is consistent with this hypothesis. If the first or second plate were generating pulses, we expect the second and/or third plate would multiply the pulses to be larger than 0.25 secondary electrons. A value of 0.25 secondary electrons would also be consistent

with continuing field emission from the dust, if the gain had decreased in the small affected region of the microchannel plates, but this would not explain the onset of the pulses when V_m is increased.

There is some indication that the damage, or some other effect of use, decreased the peak-to-valley ratio of the single-electron distribution. Nonetheless the spontaneous pulses do not seem to affect the detector's counting efficiency or background rates because typical discrimination thresholds are above the height of these pulses (sections 3.3, 3.4, and 3.5). However, we have not tested this under controlled circumstances (but see section 3.4.2). We did not find and remove the dust until we finished the controlled mass spectrometer tests.

3.7.1. Precautions to prevent damage

If V_m is turned up too quickly when the electron multiplier is first used, there is a danger that spontaneous pulses can run away and damage the microchannel plates. One experienced user told us that a high pulse rate can damage a plate in 1 msec.[56] For different electron multipliers of the same model the gain can vary by orders of magnitude at the same V_m. Therefore the timing rather than the size of the pulses is the best indicator of whether the spontaneous-pulse activity has reduced enough to continue increasing V_m.

We used a multichannel scaler to measure the timing of the the dark-noise pulses with a discrimination threshold just above the level of electronics noise. We increased V_m by 100 V increments to 1500 V and by 50 V increments to 2750 V. At each new setting there was an increase in the rate and intensity of bursts of pulses. After a few minutes to hours, the time separation of pulses approached randomness. The rule of thumb we used was to keep the largest instantaneous rates no more than a factor of ten above the average rate.

The experience with the probable damage from the discharge underscores the need for cleanliness while assembling the detector. In addition there are other precautions that might have prevented the damage. Because the microchannel-plate stack amplifies current it is the only part of the detector that is vulnerable to a moderate-size high-voltage discharge that deposits energy with a power density too small to melt metal parts. When the damage occurred, the microchannel-plate input and output voltages were at 0.4 kV and 2.7 kV respectively, each fed by a different power supply. The discharge tripped the microchannel-plate input supply, which clamped the voltage to ground. This increased V_m, initially at 2.3 kV, by up to 0.4 kV, raising the gain, which depends exponentially on V_m, by a factor of as much as five, as figure 3.3 shows. The increased gain probably exacerbated the damage that occured before the microchannel-plate output supply tripped off. The stack is also vulnerable to any other short circuits that increase V_m.

To protect the stack one can float the voltages so that one end of the stack is grounded. Then a discharge or a short circuit to ground will reduce both V_m and the gain. After the initial discharge we generally kept the microchannel-plate input grounded to avoid similar problems. One could also use external voltage dividers or other protection circuits to prevent V_m from increasing, or to prevent the current through the stack from rising above a set level, in case of a discharge. In general it might be useful to use the highest resistance and the lowest capacitance practical on all the detector leads to reduce the power released in any discharge.

4. Operating ranges

4.1. Dynamic range and upper limit on anode current

The top and bottom of the detector's dynamic range are determined by the maximum ion-count rate and the dark-noise rate respectively. The dark-noise rate is discussed in sections 3.4 and 3.5. Figure 3.10 shows that a dark rate of 10^{-4} counts/sec is possible for 40 keV ions at 50% to 70% counting efficiency. The maximum ion-count rate results from a limit on the electron-multiplier anode current. This is the current that flows from the microchannel-plate output pores to the anode. The manufacturer[36] recommends that the integrated anode current I not exceed 10% of the strip current I_s that flows through the microchannel-plate stack in its quiescent state when $I = 0$:

$$I_{max} \equiv 0.1\, I_s = 0.1\, V_m / R_m ,$$

where V_m and R_m are respectively the voltage and resistance across the microchannel-plate stack when $I = 0$.

Anode currents in excess of the nominal limit I_{max} cause substantial gain variations[27a] and, according to the manufacturer,[36] possible damage to the microchannel-plate stack. The manufacturer has run microchannel plates a factor of 100 or more above I_{max} without damage or obvious hysteresis.[36] However, others have seen hysteresis following high anode currents.[57] This electron multiplier showed hysteresis (a temporary gain decrease of 59%) following gain tests (section 3.2.2) involving high ion currents at low V_m and gains as low as unity. In these tests the anode current reached at least $I / I_{max} = 2$ and perhaps much higher. Another effect of high currents in this detector is the damage discussed in section 3.7, which was presumably caused by an excessive local current density.

We measured the decrease in this electron multiplier's gain, as a function of I / I_{max}, compared to the gain at $I = 0$. At $I / I_{max} = 0.5$ the gain is $(4 \pm 1)\%$ lower and at $I / I_{max} = 1$ the gain is $(16 \pm 2)\%$ lower. It is possible that if the ends of the

microchannel-plate stack were held directly at voltage, without the voltage-dividing low-pass filters, the gain would not decrease as much with I/I_{max}. At $V_m = 2.3\,kV$, a decrease of 1.2%, or 27 V, in the voltage across the stack could account for the 16% gain decrease (figure 3.3).

Tests by the manufacturer[36] indicate that the gain decrease as a function of I/I_{max} is affected by how much of the microchannel-plate area is being used, because the gain actually depends on the local current density. They also indicate that the gain depends on the time-averaged current for current-modulation frequencies above 100 Hz, but on the instantaneous current for frequencies below 10 Hz. We did not test either effect.

The effective resistance R across the microchannel-plate stack varies with I because the current in fired pores acts as a leakage current and the anode current from the microchannel-plate stack to the anode acts as a current shunt.[27a] When $I = 0$, R takes on the fixed value, R_m. The manufacturer measured the resistance for each of these microchannel plates before assembly. The summed resistance of the three plates stacked in series is $R_m = 2.8 \times 10^9\,\Omega$. In general this resistance varies widely from plate to plate, but each Z-stack is assembled from plates that have matched resistance. It might have been useful to monitor R_m, especially before and after exposures to air, high ion currents, or anode currents above I_{max}, for possible correlations with changes of gain. We did not monitor R_m because the high-voltage circuit made it inconvenient to do so.

The maximum anode current I_{max} determines the detector's maximum ion-count rate as follows:

$$C_{max} = I_{max} / (G_m\,\gamma\,e)\,,$$

where G_m is the electron-multiplier gain, in electrons per secondary electron; γ is the mean number of secondary electrons from the dynode collected by the microchannel plate, in

secondary electrons per ion; and e is the magnitude of the electronic charge. The dynode yield γ varies slightly with ion species, energy, and incidence angle (section 3.3.1). The microchannel-plate gain G_m increases approximately exponentially with V_m (figure 3.3). One may increase C_{max} by using a lower V_m to decrease the gain. We took advantage of this in the cyclotrino, where we increased the allowed ion count rate by operating the detector at $V_m = 2.0\,\text{kV}$ and used a preamplifier to amplify the signal.

Table 4.1 gives values for I_{max}, G_m, C_{max}, and the dynamic range, at three choices of V_m. The values were calculated using $\gamma = 23.9 \pm 0.4$ secondary electrons per ion, the value for 40 keV Cs at 82.3° incidence angle. The bottom of the dynamic range is defined to be the minimum dark-noise rate of 10^{-4} counts/sec.

Table 4.1

V_m	I_{max}	G_m	C_{max} (ion/sec)	Dynamic range	This choice of V_m achieves:
2.3 kV	82 nA	$10^{7.5}$	6.7×10^2	$10^{6.8}$	Lowest dark-noise rate.
1.6 kV	57 nA	$10^{3.7}$	2.9×10^6	$10^{10.5}$	Max ion rate in pulse-count mode.
1.2 kV	43 nA	$10^{0.3}$	5.6×10^9	$10^{13.8}$	Max ion rate in current mode.

Using the electron multiplier in the low-gain current-integrating mode prevents one from reliably discriminating ion signals from background and dark noise. However, at the high count rates that require using the current mode, background rates are not high enough to be a problem in most ion detector applications, and the total dark-noise rate of a few counts per second, typical for even low discrimination thresholds, is negligible. We have not tested whether it is feasible to use the current-integrating mode to detect large ion currents in the cyclotrino, where the background rate is much higher than in most other applications. If feasible, this might be useful for monitoring the mass 12 and 13 beams

and studying the ^{13}CH and ^{12}CH$_2$ backgrounds. Note that 5.6×10^9 ions/sec, the maximum ion count rate for $V_m = 2.3$kV, corresponds to about 1 nA of ion current. Currents approaching this size are easily measured using a Faraday cup, which might be preferable.

4.2. Recovery time, maximum background rate, and low-energy background suppression

After a group of pores in the microchannel-plate stack is fired, the recovery time to replace the stored charge in the surrounding glass is on the order of 50 to 100 msec.[26,27] If the same group of pores is fired before the charge is replaced, the gain and the resulting pulse height will be reduced.[58,59] This gain reduction is different from, and in addition to, the gain reduction discussed in section 4.1, which depends on the value of V_m.

Typically 7 adjacent pores out of a total of 1.3×10^6 are fired in the output plate of the stack (section 2.3), though additional nearby pores may also supply charge. Therefore the gain will begin to decrease as the rate of secondary electrons collected approaches 2×10^6 per second;

$$(1.3 \times 10^6 \text{ pores}) \times (7 \text{ pores/e}^-)^{-1} \times (100 \text{ msec})^{-1} = 1.9 \times 10^6 \text{ e}^-/\text{sec} .$$

This assumes the secondary electrons are distributed uniformly on average over the 1.3×10^6 pores of the input plate. If this were not true the allowed rate would be lower, depending on the particular distribution. Since the electron multiplier collects a few tens of secondary electrons for each ion, the gain will decrease as the ion rate approaches 10^4 ion/sec, again, depending on the particular distribution over the microchannel-plate face. This might require adjustment of discrimination thresholds for high count rates when the electron multiplier is in pulse-counting mode at low gain (section 4.1).

It is important that the rate of background events, which usually fire a single pore, remain well below 2×10^6 input-pores fired per second. Otherwise the background rate

could cause the gain to be reduced for ion-signal pulses. In an environment like that of the cyclotrino, with a high background flux of low-energy electrons or ions, the detector's ability to suppress low-energy background (figure 2.5) is useful for reducing the rate of pore firings due to background. For low enough energies, the electric field in the drift gap prevents even uncollimated background electrons and ions from reaching the dynode or microchannel plate and firing pores. (This effect is not to be confused with pulse-height discrimination of background after pores have been fired.) We did not test the background suppression experimentally. One could increase the background suppression by enlarging the electrodes that hold the dynode and the electron multiplier. This would increase the distance that the background must travel through the drift gap to reach the dynode and the microchannel plate.

4.3. Ion-beam size and incidence angle

The detector geometry defines a tradeoff between secondary-electron yield γ and beam width w because they both depend on the ion-incidence angle from normal, θ. For a given dynode size, the product γw is constant to first order because $w(\theta) \sim \cos\theta$ and $\gamma(\theta) \sim \sec\theta$ (sections 2.6 and 3.3.1). At $\theta = 82.3°$ the 13 mm wide dynode requires focusing the beam to 1.8 mm in one direction. A smaller incidence angle will allow a wider beam acceptance, at the expense of a lower secondary-electron yield. For this reason we use $\theta = 75°$ in the cyclotrino. We also take advantage of the 19 mm dimension of the dynode by sending the beam in through the side of the detector, which is into the page in figure 2.1. This arrangement accepts the portion of the beam that is focused to 5 mm × 13 mm, which is most of the beam.

The spot size is the area in the plane of the dynode that is intersected by the beam. One prefers to keep the spot size smaller than the dynode because secondary electrons from the edges of the dynode may not reach the microchannel plate. A spot size that does not
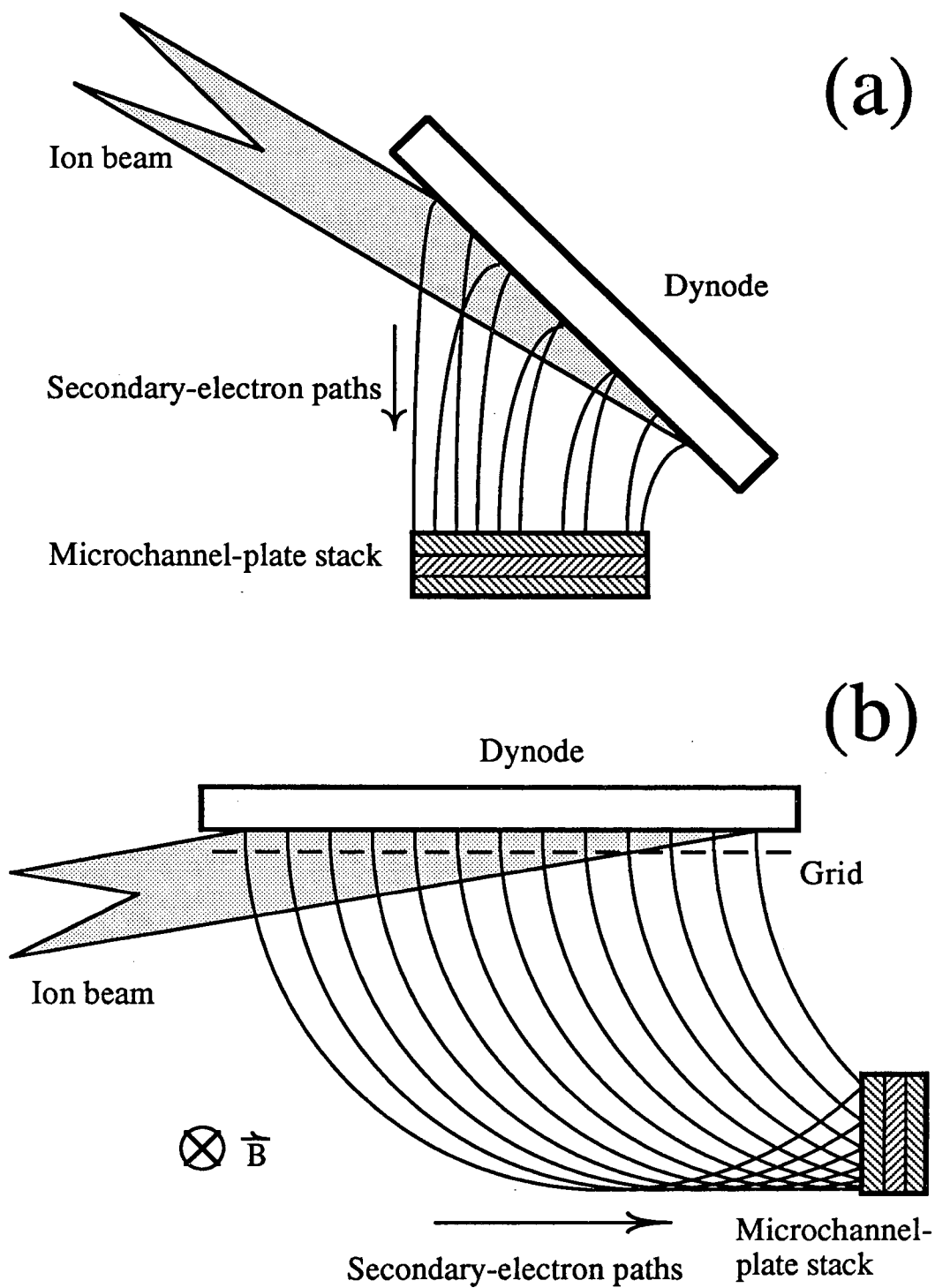
approach the edge of the dynode also makes the detector output less sensitive to beam position. But one also prefers to keep the secondary-electron yield as large as possible. Due to scattering, the yield cannot continue to increase indefinitely with θ, but angles above $82.3°$ might well be advantageous. The solution is to increase the dynode size.

While retaining the parallel geometry of the dynode and microchannel plate, the detector could be redesigned to slightly enlarge the dynode to equal the size of the 9 mm radius active area of the microchannel-plate stack. However, the parallel geometry limits the useful dynode size to that of the microchannel-plate active area. In alternative designs this limit could be overcome by focusing the secondary electrons from the dynode onto the microchannel plate. This might be achieved by using focusing elements or merely by placing the dynode at an angle to the microchannel-plate stack as shown in figure 4.1(a). If the dynode and microchannel plate were mounted at right angles to one another, a magnetic field could be used to focus the secondary electrons from a larger dynode onto the microchannel-plate active area. This would require a grid to accelerate the secondary electrons in order to reduce their relative momentum scatter, as shown in figure 4.1(b). The field could be supplied by two small permanent magnets, or perhaps by the cyclotron fringe field. One might also use an electron multiplier with a larger active area. Microchannel plates with dimensions above 10 mm are now available.

4.4. Operating pressures

Siegmund et al[55] have operated Z-stack electron multipliers at pressures from 7×10^{-7} Torr to 1.5×10^{-5} Torr and found no change in the background rate over that range. The manufacturer expects that there may be problems with microchannel-plate gain stability or aging at or above pressures in the 10^{-6} or 10^{-5} Torr range.[36] Aging refers to changes in electron-multiplier behavior, especially gain, which depend on the total integrated charge extracted during the electron multiplier's lifetime.[43] The manufacturer

(a)

Ion beam

Dynode

Secondary-electron paths

Microchannel-plate stack

(b)

Dynode

Grid

Ion beam

$\otimes \; \vec{B}$

Secondary-electron paths

Microchannel-plate stack

Figure 4.1   These two illustrations of arrangements for increasing the dynode size relative to the microchannel-plate active area are discussed in section 4.3.

does not expect microchannel plates to work at 10^{-3} Torr. We have tested the detector in the cyclotrino at pressures up to about 2×10^{-7} Torr with no apparent change in behavior. Most of the data presented in this work were taken at the mass-spectrometer base pressure of 1 to 3×10^{-9} Torr.

4.5. Sensitivity to magnetic fields

The microchannel-plate stack is insensitive to magnetic fields of up to about 2 kilogauss along the pores, and at least 1 kilogauss in the perpendicular direction. This is due to the small pore size and the strong electric field within the pores.[50] However, the detector as a whole is sensitive to magnetic fields that are strong enough to deflect secondary electrons in the drift gap. We analyze separately the effects of magnetic fields that are perpendicular and parallel to the electric field in the drift gap.

A perpendicular magnetic field in the drift gap displaces the collection point for each secondary electron in a direction parallel to the microchannel-plate face. This is true as long as the magnetic field B is not too much stronger than the electric field E, in Gaussian units. We operate with $E = 1$ kV/cm, or 3.3 statvolts/cm, an equivalent field strength to 3.3 gauss. If the magnetic field is too strong the electrons will return to the dynode without reaching the microchannel plate. The standard method for analyzing perpendicular E and B fields is to transform to the frame in which the smaller field vanishes. We take the case $B > E$ because the displacement is greater than for $B < E$. In the transformed frame the electron path is a circle, which transforms back to a cycloid in the lab frame. To first order, the displacement d depends on B and on the distance s and the voltage V_d across the drift gap, as $d \sim B s^2 (V_d)^{-1/2}$. For $B = 10$ gauss the displacement is 0.6 mm at the plane of the field wires. Beyond the field wires $E = 0$ so the path is circular with an 11 cm radius. The displacement at the microchannel-plate face is about 1 mm. A much larger displacement would substantially reduce the effective size of the dynode.

A parallel magnetic field will cause the secondary-electron paths to be helical around an axis normal to the dynode. The helix radius depends on the initial energy and direction of each secondary electron emitted from the dynode. Thus if B is too strong the radii of the secondary electrons ejected by an ion will be too small for the electrons to separate sufficiently from one another to be independently multiplied in the microchannel-plate stack (section 2.7.1). The result would be a lower effective gain for ion-signal pulses. We do not know what separation is required for independent multiplication, but the present separation appears to be sufficient. In order to calculate an upper limit on B for which the gain reduction is negligible, we impose the condition that the electrons must complete less than one-half orbit before they hit the microchannel plate. This will maintain nearly the present separation. The time of flight is 1.4 nsec. The B field has a larger effect on electrons with lower initial transverse energies. We take 1 eV as the initial transverse energy in order to find an upper limit on B since most of the electrons have higher energies[35] and are effected less strongly by the B field. Setting the time of flight equal to one half of the orbital period for a 1 eV electron yields an upper limit on B of 110 gauss. This limit ensures that the separation of the secondary electrons at the microchannel-plate face would not be reduced, so any gain reduction would be negligible.

For a B field of unknown direction the possibility that the fields are perpendicular limits B to the order of 10 gauss. In the mass spectrometer the field at the detector was 3 or 4 gauss in an unknown direction. The detector showed no adverse effects. In the cyclotrino, 0.25 inch thick steel shielding (figure 1.1) reduces the measured magnetic field at the detector, immediately outside the magnet poles, to about 5 gauss. The field is approximately parallel to the electric field in the drift gap. This field also causes the detector no problems as far as we can tell. In applications where magnetic shielding could not be used to reduce the magnetic field to acceptable levels, other possible solutions are to

increase V_d or decrease the distance from the dynode to the microchannel plate. For a transverse magnetic field the dynode can be offset with respect to the microchannel plate to correct for the magnetic deflection. The detector's dovetailed dynode slot makes this a straightforward adaptation.

4.6. Uniformity of response over microchannel-plate and dynode surfaces

In the cyclotrino we are trying to achieve high sensitivity but we expect the accuracy of abundance-ratio measurements to be limited by statistics and systematics that are not attributable to the detector. However, in other applications to mass spectrometry, high accuracy requires detectors that among other things are insensitive to incident ion-beam position. This prevents small errors in the magnetic field from causing errors in measured isotope ratios when sweeping through the mass spectrum or switching between beams of different masses. In such applications it is important that both the dynode and the microchannel-plate stack have uniform response over their surfaces. Otherwise the counting efficiency at a given discrimination threshold will vary depending on where ions hit. This would introduce errors in the measured abundance. Dietz[30] concludes that the Al_2O_3 dynodes he has made and tested have no differences in observed secondary-electron emission over their area.

Manufacturer tests of image intensifiers show that there are no Moiré patterns in the output of stacked microchannel plates stimulated by uniform input from photocathodes.[36,38,39] This indicates that neither pore alignment between plates in the stack (section 2.3), nor differences in collection efficiency between the webbing and the pores, cause observable gain variations over the active area. The absence of other observed variations in gain across the active area in these tests indicates the absence of other possible causes of gain variation, such as uneven gaps between plates, which would allow pores in some portions of one plate to fire larger numbers of pores in the next plate.

Section 2.7.2 quotes limits on collection-efficiency variations over the active area. In the detector, we expect gain variations on a scale smaller than 1 mm to average out because the secondary electrons from a single ion fire pores over a larger distance than 1 mm (section 2.7.1). If the gain uniformity over the microchannel-plate area were found to be insufficient for some application, one might try using an electron multiplier with a microchannel-plate stack that had been electron scrubbed (section 3.2.2).

In practice, insensitivity to position can be achieved only if the beam is substantially smaller than the dynode. In the tests in both the mass spectrometer and the cyclotrino, the beam emittance and the grazing-incidence angle caused some of the ions to hit near or beyond the edge of the dynode. This prevented us from testing whether the detector would be sensitive to beam position within the dynode. We expect that for a spot size smaller than the dynode a uniform response could be achieved.

5. Conclusion

The detector has successfully proved it can discriminate the signal of a full-energy ion from the actual background in the operating cyclotrino. There the detector has enabled us to reach the low background rate of 6×10^{-4} counts/sec with 50% counting efficiency for 36 keV ions. The detector has in turn been used to test the cyclotrino tail rejection.[8] The small mass difference of 1/1800 between ^{14}C and ^{13}CH requires that the background transmission fall from its maximum value by 8 to 11 orders of magnitude when we change the tuning frequency by 1/1880. Experiments show that the combination of the detector and the cyclotrino reduce the background transmission by a factor of 2×10^{11} in less than the required frequency change. This will enable us to date 30,000 year old milligram samples of carbon with less than 10% statistical uncertainty in the $^{14}C/^{12}C$ ratio.

We expect that the detector's insensitivity to beam position will also be advantageous for standard mass spectrometry, in which accurate isotope-ratio measurements require insensitivity to beam-position errors. The detector's performance in reducing background should also be useful in general ion detection and mass spectrometry. The dark noise is 10^{-4} counts/sec for counting 40 keV ions with 50% to 70% efficiency, or 10^{-2} counts/sec for counting 5 keV ions with about 50% efficiency. This makes it possible to detect trace elements or isotopes at at similar low rates. This can facilitate standard mass spectrometry on small, perhaps hand-picked, samples. We have shown that the detector can reduce low-energy background by factors of 10^2 to 10^4 at discrimination thresholds that allow a counting efficiency of 99% for 40 keV ions or about 50% for 5 keV ions. This should allow low-rate *in situ* detection of trace ions in environments with high background rates.

We will soon install the higher-current external ion source on the cyclotrino. This will allow us to date real samples. The data we have obtained with the detector in the cyclotrino indicate that with four orders of magnitude more beam current the background

References

1. G. M. Raisbeck and F.Yiou, "Production of long-lived cosmogenic nuclei and their applications," *Nucl. Instrum. Methods* **B5** (2) 91-99 (1984).

2. L. W. Alvarez, "The early days of accelerator mass spectrometry," in Proceedings of the Symposium on Accelerator Mass Spectrometry, Argonne National Lab Report ANL/PHY-81-1 (1981) pp.1-15.

3. R. A. Muller, "Radioisotope dating with a cyclotron," *Science* **196**, 489-484 (1977).

4. E. J. Stephenson, T. S. Mast, and R. A. Muller, "Radiocarbon dating with a cyclotron," *Nucl. Instrum. Methods* **158** 571-577 (1979).

5. A. E. Litherland, "Accelerator mass spectrometry," *Nucl. Instrum. Methods* **B5** (2) 162-166 (1984).

6. D. J. Donahue, A. J. T. Jull, and T. H. Zabel, "Results of radioisotope measurements at the NSF-University of Arizona tandem accelerator mass spectrometer facility," *Nucl. Instrum. Methods* **B5** (2) 162-166 (1984).

7. W. G. Mook, "Achaeological and geological interest in applying ^{14}C AMS to small samples," *Nucl. Instrum. Methods* **B5** (2) 297-302 (1984).

8. J. J. Welch, K. J. Bertsche, P. G. Friedman, D. E. Morris, R. A. Muller, and P. P. Tans, "A low energy cyclotron for radiocarbon dating," to be published in *Nucl. Instrum. Methods B.*

9. R. A. Muller, P. P. Tans, T. S. Mast, and J. J. Welch, "Mass spectrometry with a very small cyclotron," in Proceedings of the Symposium on Accelerator Mass Spectrometry, Argonne National Lab Report ANL/PHY-81-1 (1981) pp. 342-345, also published as LBL-12797, Lawrence Berkeley Laboratory.

10. J. J. Welch, K. J. Bertsche, P. G. Friedman, D. E. Morris, and R. A. Muller, "Advanced accelerator methods: the cyclotrino," Accelerator mass spectrometry workshop held in Irvine, CA 15 Feb 1986.

11. R. Middleton, "A versatile high intensity negative ion source," *Nucl. Instrum. Methods* **220** 105-106 (1984).

12. D. E. Morris, "A new method for injecting charged particles across a magnetic field," *Nucl. Instrum. Methods* **A248** 279-300 (1986).

13. J. J. Welch, "A low energy cyclotron for radiocarbon dating," Ph.D. thesis, University of California, Berkeley (1984), Lawrence Berkeley Laboratory report LBL-21255.

14. L. C. Northcliffe and R. F. Schilling, "Range and stopping-power tables for heavy ions," *Nucl. Data Tables* **A7** (3&4) 233-463 (1970); This and the following two references may be used to extrapolate an approximate upper limit of 1000 Å for the range of 36 keV ^{14}C in Al_2O_3.

15. B. Domeij, F. Brown, J. A. Davies, and M. McCargo, "Ranges of heavy ions in amorphous oxides" *Can. J. Phys.* **42** (8) 1624-1634 (1964).

16. D. C. Santry and C. W. Sitter, "Range and retention of 40 keV ions in solids," in Proceedings of the International Conference on Electromagnetic Isotope Separators and Techniques of their Application, held in Marburg, Sept. 7-10, 1970, edited by H. Wagner and W. Walcher (Zentralstelle fur Atomkernenergie - Dokumentation (ZAED), 7501 Leopoldshafen, Kernforschungszentrum, (1970) 505-524.

17. L. A. Dietz and L. R. Hanrahan, "Electron multiplier-scintilator detector for pulse counting positive or negative ions," *Rev. Sci. Instrum.* **49** (9), 1250-1256 (1979).

18. A. B. Hance, Knolls Atomic Power Laboratory, Schenectady, NY (private communication).

19. L. A. Dietz, L. R. Hanrahan, and A. B. Hance, "Fabrication of 18-stage electron multiplier," KAPL-3352, Knolls Atomic Power Laboratory, Schenectady, NY (Jun 1967).

20. N. R. Daly, "Scintillation type mass spectrometer ion detector," *Rev. Sci. Instrum.* **31** (3), 264-267 (Mar 1960).

21. B. W. Ridley, "A large aperture detector for slow positive ions," *Nucl. Instrum. Methods* **14** 231-236 (1961).

22. J. L. Wiza, "Microchannel plate detectors," *Nucl. Instrum. Methods* **162**, 587-601 (1979).

23. B. Leskovar, "Microchannel plates," *Physics Today* **30** (11) 42-49 (Nov 1977).

24. G. W. Fraser, "X- and γ-ray imaging using microchannel plates," *Nucl. Instrum. Methods* **221**, 115-130 (1984).

25. S. Dhawan, "Introduction to microchannel plate photomultipliers," *IEEE Trans. Nucl. Sci.* **NS-28** (1) 672-676 (1981).

26. E. H. Eberhardt, "Parameters pertaining to microchannel plates and microchannel plate devices," ITT/EOPD Technical Note No.127, ITT Electro-optical Products Division, 3700 East Pontiac Street, Fort Wayne, IN 46803 (Aug 1980).

27. C. C. Lo and B. Leskovar, "Performance studies of high gain photomultiplier having Z-configuration of microchannel plates," *IEEE Trans. Nucl. Sci.* **NS-28** (1) 698-704 (Feb 1981).

27a. S. Matsuura, S. Umebayashi, C. Okuyama, and K. Oba, "Current status of the microchannel plate," *IEEE Trans. Nucl. Sci.* **NS-31** (1) 399-403 (Feb 1984).

28. H. Bruining, *Physics and applications of secondary electron emission* (Pergamon Press, New York) p. 39.

29. L. A. Dietz (private communication).

30. L. A. Dietz and J. C. Sheffield, "Secondary electron emission induced by 5 - 30 keV monotonic ions striking thin oxide films," *J. Appl. Phys.* **46** (10) 4361-4370 (Oct 1975).

31. L. A. Dietz, "Basic properties of electron multiplier ion detection and pulse counting methods in mass spectrometry," *Rev. Sci. Instrum.* **36** (12) 1763-1771 (Dec 1965).

32. K. H. Krebs, "Electron ejection from solids by atomic particles with kinetic energy," *Fortschr. Phys.* **16**, 419-490 (1968). This is a large review article.

33. L. A. Dietz and J. C. Sheffield, "Spectrometer for measuring secondary electron yields by ion inpacts on thin film oxide surfaces," *Rev. Sci. Instrum.* **44** (2) 183-191 (Feb 1973).

34. G. Carter and J. S. Colligon, *Ion Bombardment of Solids* (American Elsevier, New York, 1968) p. 52.

35. M. Kaminsky, *Atomic and Ionic Phenomena on Metal Surfaces* (Academic Press, New York, 1965) pp. 329-331.

36. E. H. Eberhardt (private communication).

37. R. C. Taylor, M. C. Hettrick, and R. F. Malina, "Maximizing the quantum efficiency of microchannel plate detectors: The collecton of photoelectrons from the interchannel web using an electric field," *Rev. Sci. Instrum.* **54** (2), 171-176 (Feb 1983).

38. O. H. W. Siegmund, M. Lampton, J. Bixler, S. Boyer, and R. F. Malina, "Operational Characteristics of wedge and strip readout systems," *IEEE Trans. Nucl. Sci.* **33** (1) 724-727 (Feb 1986).

39. O. H. W. Siegmund, M. Lampton, S. Chakrabarti, J. Vallerga, S. Boyer, and R. F. Malina, "Application of wedge and strip readout systems to detectors for astronomy," *SPIE Proceedings* **627** (1986).

40. O. H. W. Siegmund, (private communication, 1986).

41. E. H. Eberhardt (unpublished).

42. J. G. Timothy, "Curved-channel microchannel array plates, " *Rev. Sci. Instrum.* **52** (8) 1131-1142 (1981).

43. R. F. Malina and K. R. Coburn, "Compatative lifetesting results for microchannel plates in windowless EUV photon detectors," *IEEE Trans. Nucl. Sci.* **NS-31** (1) 404-407 (Feb 1984).

44. E. H. Eberhardt, "Gain model for microchannel plates," *Appl. Opt.* **18** (9) 1418-1423 (May 1979).

45. E. H. Eberhardt, "An operational model for microchannel plate devices," *IEEE Trans. Nucl. Sci.* **NS-28** (1) 712-717 (Feb 1981).

46. N. R. Daly and R. E. Powell, "Relative secondary electron coefficients for 40 keV noble gas and alkali metal ions of aluminum," *Proc. Phys. Soc.* **84**, 595-598 (1964).

47. B. L. Schram, A. J. H. Boerboom, W. Klein, and J. Kistemaker, "Amplification factors of a particle multiplier for multiply charged noble gas ions," *Physica* (Utrecht), **32** (4) 749-761 (1966).

48. M. L. Meade, "Instrumentation aspects of photon counting applied to photometry," *J. Phys. E* (GB) **14** (8) 909-918 (Aug 1981). Review article.

49. *Photomultiplier Handbook*, RCA, Solid State Division, Electro Optics and Devices, Lancaster, PA 17604.

50. K. Oba and P. Rehak, "Studies of high-gain microchannel plate photo-multipliers," *IEEE Trans. Nucl. Sci.* **NS-28** (1) 683-688 (Feb 1981).

51. J. R. Prescott, "A statistical model for photomultiplier single-electron statistics," *Nucl. Instrum. Methods* **39**, 173-179 (1966).

52. L. A. Dietz, "Use of Polya statistics in investigations of secondary electron yields from target surfaces," *Rev. Sci. Instrum.* **38** (9) 1332-1333 (Sep 1967).

53. L. A. Dietz, L. R. Hanrahan, and A. B. Hance, "Single-electron response of a porous KCl transmission dynode and application of Polya statistics to particle counting in an electron multiplier," *Rev. Sci. Instrum.* **38** (2) 176-183 (Feb 1967).

54. L. A. Dietz, "General method for computing the statisics of charge amplification in particle and photon detectors used for pulse counting," *Int. J. Mass Spectrom. Ion Phys.* **5** (1&2) 11-19 (1970).

55. O. H. W. Siegmund, R. F. Malina, K. Coburn, and D. Werthimer, "Microchannel plate EUV detectors for the extreme ultraviolet explorer," *IEEE Trans. Nucl. Sci.* **NS-31** (1) 776-779 (Feb 1984).

56. Norm Madden, Lawrence Berkeley Laboratory (private communication).

57. *Characteristics and applications of microchannel plates,* Technical manual Res-0795, Hamamatsu Corporation, 420 South Avenue, Middlesex, NJ 08846.

58. O. H. W. Siegmund, K. Coburn, and R. F. Malina, "Investigation of large format microchannel plate Z configurations," *IEEE Trans. Nucl. Sci.* **NS-32** (1) 443-447 (Feb 1985).

59. E. B. Nieschmidt, R. S. Lawrence, and C. D. Gentillon, "Count rate performance of a microchannel plate photomultiplier," *IEEE Trans. Nucl. Sci.* **NS-29** (1) 196-199 (Feb 1982).

Each year the first issue (Feb) of *IEEE Trans. Nucl. Sci.* contains the papers given at the Nuclear Science Symposium which include several articles on microchannel plates and their applications. These are listed under such section headings as Photo-multipliers and optical detectors, Space instrumentation, and Detectors.